Estuaries and Coasts (2021) 44:972–990
https://doi.org/10.1007/s12237-020-00840-y

Suspended-sediment Flux in the San Francisco Estuary; Part II: the Impact of the 2013–2016 California Drought and Controls on Sediment Flux

D. N. Livsey[1] · M. A. Downing-Kunz[1] · D. H. Schoellhamer[1] · A. Manning[2,3,4,5]

Received: 24 October 2019 / Revised: 17 September 2020 / Accepted: 25 September 2020 / Published online: 2 November 2020
© This is a U.S. government work and not under copyright protection in the U.S.; foreign copyright protection may apply 2020

Abstract
Recent modeling has demonstrated that sediment supply is one of the primary environmental variables that will determine the sustainability of San Francisco Estuary tidal marshes over the next century as sea level rises. Therefore, understanding the environmental controls on sediment flux within the San Francisco Estuary is crucial for optimal planning and management of tidal marsh restoration. Herein, we present suspended-sediment flux estimates from water year (WY) 2009–2016 from the San Francisco Estuary to investigate the environmental controls and impact of the record 2013–2016 California drought. During the recent drought, sediment flux into Lower South Bay, the southernmost subembayment of the San Francisco Estuary, increased by 345% from 114 kt/year from WY 2009 to 2011 to 508 kt/year from WY 2014 to 2016, while local tributary sediment flux declined from 209 to 51 kt/year. Total annual sediment flux from WY 2009 to 2011 and 2014 to 2016 can be predicted by total annual freshwater inflow from the Sacramento-San Joaquin Delta ($R^2 = 0.83$, $p < 0.01$), the primary source of freshwater input into the San Francisco Estuary. The volume of freshwater inflow from the Sacramento-San Joaquin Delta is hypothesized to affect shoal-to-channel density gradients that affect sediment flux from broad, typically more saline and turbid shoals, to the main tidal-channel seaward of Lower South Bay. During the drought, freshwater inflow from the Sacramento-San Joaquin Delta decreased, and replacement of typically more saline shoal water was reduced. As a result, landward-increasing cross-channel density gradients enhanced shoal-to-channel advective flux that increased sediment available for tidal dispersion and drove an increase in net-landward sediment flux into Lower South Bay.

Keywords Estuarine processes · Suspended-sediment · Sediment supply · Cohesive sediment · Flocculation · San Francisco Estuary

Introduction

Tidal marshes are habitats with a diverse array of flora and fauna and provide a wide range of ecosystem services to urban areas such as wildlife, recreation, and education resources, storm and flood protection, and pollution reduction (Costanza et al. 1997). Globally, over the last 300 years more than 65% of wetland habitats have been lost to resource over-use, development, and pollution (Boesch et al. 2001; Jackson et al. 2001; Lotze et al. 2006). Within the San Francisco

Communicated by Neil Kamal Ganju

✉ D. N. Livsey
livsey.daniel@gmail.com

M. A. Downing-Kunz
mdowning-kunz@usgs.gov

D. H. Schoellhamer
dschoell@usgs.gov

A. Manning
andymanning@yahoo.com

[1] California Water Science Center, U.S. Geological Survey, 6000 J Street, Placer Hall, Sacramento, CA 95819-6129, USA

[2] Coasts & Oceans Group, HR Wallingford Ltd., Wallingford OX10 8BA, UK

[3] Energy & Environment Institute, University of Hull, Hull HU6 7RX, UK

[4] Department of Civil and Environmental Engineering, Stanford University, Stanford, CA 94305, USA

[5] School of Biological and Marine Sciences, University of Plymouth, Plymouth PL4 8AA, UK

Estuary (SFE), the second largest estuary on the western coast of the Americas, 80% of the historic tidal marsh habitat, 60,000 ha, has been lost (Lotze et al. 2006). In the southernmost subembayment of the SFE, the South Bay Salt Ponds Restoration Project aims to restore 6000 ha of subsided, leveed salt ponds into tidal marsh and managed wetland (Fig. 1). Recent modeling has demonstrated that sediment supply is one of the primary environmental variables that will determine the sustainability of SFE tidal marshes over the next century as sea level rises (Stralberg et al. 2011; Swanson et al. 2014). Therefore, understanding the environmental controls on sediment flux within the SFE is crucial for optimal planning and management of tidal marsh restoration.

Shellenbarger et al. (2013) collected and analyzed sediment flux data in Lower South Bay, a subembayment of the SFE, near the South Bay Salt Ponds Restoration Project during water years (WY, defined as October 1 of the previous calendar year to September 30) 2009–2011. We build upon this work with 3.5 additional years of sediment flux data, collected during the recent, record-breaking drought in California during WY 2013–2016 (Livsey et al. 2020). From WY 2013–2016 California experienced the worst drought in the instrumental record (Robeson 2015) with record-high salinity and temperature observed in the SFE (Work et al. 2017). In this study, changes in interannual suspended-sediment flux estimates are utilized to investigate the controls on sediment flux in the SFE and the impact of the recent California drought on sediment flux in the SFE. A conceptual model is developed to demonstrate how decreases in freshwater inflow can lead to increased sediment flux into an estuarine subembayment.

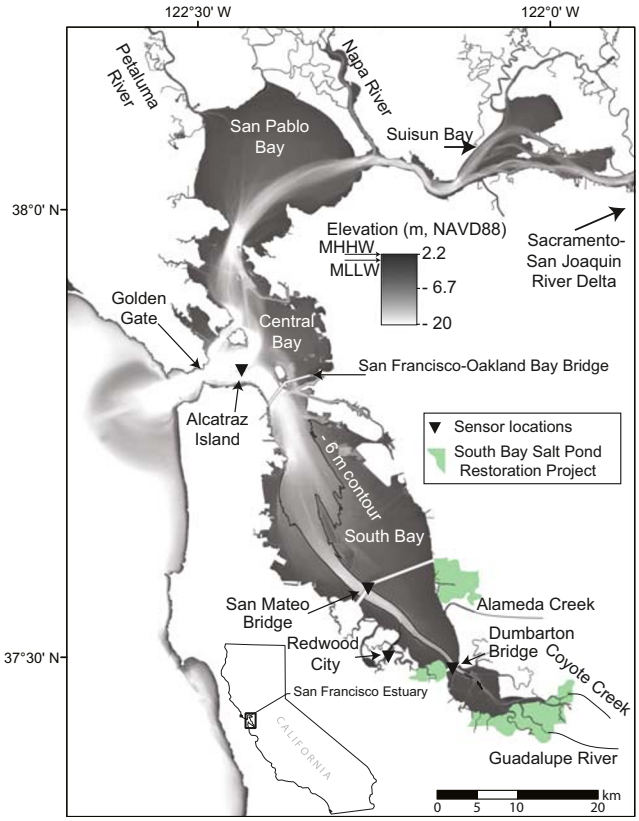

Fig. 1 San Francisco Estuary with subembayments, major tributaries, and locations of referenced sensors at Dumbarton Bridge (USGS station ID 373015122071000) San Mateo Bridge (USGS station ID 11162765), Alcatraz Island (USGS station ID 374938122251801), and Redwood City (NOAA Station 9414523). Bathymetry data, referenced from North American Vertical Datum 1988 (NAVD88), are from NOAA (2010). Elevation of mean lower low water (MLLW) and (MHHW) at Dumbarton Bridge, estimated from NOAA (2019), is − 0.4 m and − 2.2 m from NAVD88, respectively. Contour at − 6 m in South Bay is utilized as boundary between main tidal channel and shoals. Note maximum tidal excursion at Dumbarton Bridge is 14 km, distance from stations at Dumbarton Bridge to San Mateo Bridge is 14.6 km. Basemap generated from data from NOAA (1998)

Study Area

Based on general circulation patterns, the SFE can be broadly divided into northern and southern regions divided by the San Francisco-Oakland Bay Bridge (Walters et al. 1985). North of the San Francisco-Oakland Bay Bridge, Central Bay, forms the seaward boundary of South Bay with the seaward boundary of the SFE at the Golden Gate (Fig. 1). South Bay is defined as the SFE between the San Francisco-Oakland Bay Bridge and Dumbarton Bridge (Fig. 1). Lower South Bay (LSB) is the southernmost subembayment of the SFE and is defined as the SFE south of Dumbarton Bridge (Fig. 1). In embayments north of the San Francisco-Oakland Bay Bridge, freshwater inflow from the Sacramento-San Joaquin Delta ("Delta") and saline ocean water entering from the Golden Gate form circulation patterns consistent with a partially mixed estuary (Fig. 1; Dyer 1998). In South Bay and LSB, freshwater inflow from the Delta enters at the seaward boundary of the subembayments and results in circulation patterns characteristic of a "tidally oscillating lagoon" with exchange of salt and sediment between South Bay and Central Bay controlled primarily by baroclinic residual flows (McCulloch et al. 1970; Conomos 1979; Conomos et al. 1985; Walters et al. 1985; Largier et al. 1997; Kimmerer 2002; Gostic 2018).

For the SFE, 93% of the freshwater flow and 39% of suspended-sediment supply enters from the Delta (McKee et al. 2013; Fig. 1). The timing of freshwater inflow from the Delta varies by year, but most of the inflow occurs in the winter-spring (Nov–May) wet season (Kimmerer 2002). Freshwater inflow from the Delta from November to February is driven by precipitation in the watershed, while freshwater inflow from March to May is driven by snowmelt in the Sierra Nevada (Kimmerer 2002). During dry years, freshwater inflow from the Delta is reduced but is still orders of magnitude greater than freshwater inflow from local tributaries (McKee et al. 2013). Freshwater inflow from the Delta controls the wet-season reduction in salinity throughout the

SFE with salinity at LSB decreasing approximately 2 weeks after peak freshwater inflow (McCulloch et al. 1970; Shellenbarger and Schoellhamer 2011).

The bathymetry of the SFE is characterized by a channel-shoal geometry with a main tidal-channel flanked by shoals (Fig. 1). The main channel in LSB and South Bay is less than 1 km wide. Shoals in LSB reach up to 3 km in width on each side of the channel, while the shoals north of Dumbarton Bridge can extend up to 10 km in width (Fig. 1). At mean tide level, LSB mean water depth and surface area are 2.6 m and 34 km^2, respectively (Hager and Schemel 1996). Maximum water depth in LSB is 20 m, and the mixed semidiurnal tidal range is approximately 3 m (Shellenbarger et al. 2013). Maximum depth-averaged tidal velocity at Dumbarton Bridge reaches 1 m/s (Shellenbarger et al. 2013) and is flood dominant (Elias et al. 2013; Livsey et al. 2020). Freshwater inflow from the Delta is preferentially dispersed in South Bay from the main channel to the shoals because freshwater inflow from the Delta enters South Bay on the flood tide and the maximum along-channel tidal excursion in the main channel is on the order of 10 km, while the maximum along-channel and cross-channel tidal excursion on the shoals is on the order of 1–5 km (Powell et al. 1989; Lacy et al. 2014).

Suspended-sediment concentration (SSC) at Dumbarton Bridge is mostly influenced by spring-neap tidal variation in current velocity, advection of resuspended shoal sediment on ebb tide, and seasonal variability in wind speed, rather than freshwater inflow from local tributaries (Schoellhamer 1996; Shellenbarger et al. 2013; Gostic 2018). During spring tides, current velocity in the channel reaches 1 m/s leading to increased resuspension by tides compared with neap tides with maximum velocity typically around 0.75 m/s. Maxima in SSC occur on ebb tides after peak ebb velocity and have been attributed to advection of resuspended shoal sediment into the main channel (Schoellhamer 1996; Crauder et al. 2016). For most of the year, the wind over LSB is from the northwest with a diurnal cycle. Monthly median wind speeds, computed for WY 2009–2011 and WY 2013–2016 from observations at Redwood City, CA (NOAA Station 9414523; Fig. 1), increase from March (~ 2 m/s) to April (~ 4 m/s) and remain relatively high (> 3 m/s) until they decrease from September (~ 3 m/s) to October (~ 1.5 m/s). Sediment concentrations over the shoals of South Bay tend to be higher on flood tide compared with ebb tide due to propagation of a standing wave along the axis of South Bay and enhanced wind-wave resuspension during low water level (Lacy et al. 1996). Most variability in wind direction occurs from October to March due to storm-related winds from the south (Brand et al. 2010).

Based on other studies of suspended-sediment transport in the SFE (e.g., Ganju and Schoellhamer 2006; Downing-Kunz and Schoellhamer 2013), the controls of residual, tidally averaged, suspended-sediment flux at Dumbarton Bridge are expected to be advection, tidal dispersion, and Stokes drift due to the tidal wave propagation. In the "Methods" section we utilize the decomposition of Dyer (1974) to quantify each of these terms in the residual, tidally averaged, suspended-sediment flux at Dumbarton Bridge. Below we provide a brief description of each term and describe possible drivers of seasonal and interannual change in each term.

Estuarine advective flux is the subtidal transport of sediment mediated by the estuarine circulation that drives subtidal, along-channel (x-coordinate, landward positive) and cross-channel (i.e., channel-to-shoal, y-coordinate, landward positive) flow (Geyer and MacCready 2014). The estuarine circulation is affected by gradients in water density (ρ), tidal straining, and bathymetry (Geyer and MacCready 2014). Because along-channel flow and cross-channel flow between the channels and shoals are important drivers of advective flux in the SFE (e.g., Lacy et al. 2014; Gostic 2018), subtidal flow is delineated between along-channel exchange flow and cross-channel exchange flow. For much of the year, there is a landward along-channel exchange flow (i.e., net inflow of bottom water and net outflow of surface water) driven by a typical (negative) estuarine density gradient (i.e., $\delta\rho/\delta x$ decreasing in the landward direction) from Central Bay to LSB (Conomos et al. 1985; Gostic 2018). Landward, along-channel exchange flow is thought to drive net-landward advective flux towards LSB (Gostic 2018). Cross-channel exchange flow between the channels and shoals is thought to be typically channelward (i.e., net channel-directed outflow of bottom water and net shoal-directed inflow of surface water) because freshwater from the Delta is preferentially dispersed along the main-tidal channel (Pubben 2017). Channelward cross-channel exchange flow enhances advective flux from more turbid shoals to the main tidal channel (Lacy et al. 2014).

Along-channel and cross-channel exchange flow in LSB and South Bay is primarily controlled by changes in freshwater inflow from the Delta between the wet and dry seasons (McCulloch et al. 1970; Walters et al. 1985; Powell et al. 1989; Pubben 2017; Gostic 2018). At the onset of freshwater inflow from the Delta, during the rising limb of the hydrograph, landward along-channel exchange flow is weakened because freshwater inflow from the Delta enters at the seaward boundary of South Bay (Gostic 2018). Seaward along-channel exchange flow (i.e., net outflow of bottom water and net inflow of surface water) may occur as freshwater inflow from the Delta induces a positive $\delta\rho/\delta x$ from Central Bay to LSB (i.e., an increase in density in the landward direction). Periods of seaward along-channel exchange flow occur on time-scales of days with net-seaward advective flux and sediment export from LSB (Walters et al. 1985; Gostic 2018). Approximately 2 weeks after the peak in freshwater inflow from the Delta, during the falling limb of the hydrograph, LSB salinity reduces, and landward along-channel exchange flow is enhanced from October to April (McCulloch et al. 1970; Walters et al. 1985; Shellenbarger and Schoellhamer

2011; Pubben 2017). The strength and direction of cross-channel exchange flow depend on the volume of freshwater inflow from the Delta (Pubben 2017). At the onset of freshwater inflow, positive cross-channel density gradients ($\delta\rho/\delta y$ increasing in the landward direction) increase; however, with sufficient freshwater inflow, saline shoal water is replaced, and positive $\delta\rho/\delta y$ weakens, and may become negative (Powell et al. 1989; Lacy et al. 2014).

During the dry season (July–September), freshwater from the Delta in South Bay is replaced by saline ocean water (van Kempen 2017), the magnitudes of negative $\delta\rho/\delta x$ and positive $\delta\rho/\delta y$ are minimized (Pubben 2017), and salinity in South Bay increases in response to increasing evaporation (McCulloch et al. 1970; Largier et al. 1997). When salinity in South Bay exceeds salinity in Central Bay an estuarine circulation characteristic of a "low-inflow" estuary occurs (Largier et al. 1997). Along-channel exchange flow when salinity in South Bay exceeds salinity in Central Bay is thought to trap sediment in LSB through the development of landward, along-channel exchange flow and net-landward advective flux towards LSB (McCulloch et al. 1970; Largier et al. 1997). Although positive $\delta\rho/\delta y$ are near zero, channelward cross-channel exchange flow and shoal-to-channel sediment flux can be enhanced when water over the shoals is more turbid and cooler than channel water (Lacy et al. 2014).

Tidal dispersion is the flux arising from correlations between tidally fluctuating velocity and sediment concentration (Geyer and Signell 1992). In the SFE, SSC generally decreases moving seaward from LSB to Central Bay, except when turbid freshwater inflow from the Delta enters Central Bay (McCulloch et al. 1970). Analysis of SSC estimates from Buchanan et al. (2018) collected at Dumbarton Bridge and at Alcatraz Island in Central Bay indicates tidally filtered SSC was always higher at Dumbarton Bridge than Alcatraz Island from WY 2009 to 2016. Therefore, tidal dispersion along the channel of South Bay for much of the year is expected to be directed seaward. That said, local reversals in the positive along-channel SSC gradient (δSSC/δx increasing in the landward direction) could develop from transport of resuspended shoal sediment into the main channel and input of tributary-derived sediment. For example, transport of resuspended, shoal-derived sediment into the main channel at the end of ebb tide (Schoellhamer 1996), wind-driven return flows induced by sustained (> 24 h) winds (Brand et al. 2010), and/or enhanced channelward cross-channel exchange flow (Lacy et al. 2014) may result in seaward-increasing δSSC/δx and net-landward dispersive flux. Tributary derived sediment may induce local maxima in suspended sediment concentrations north or south of Dumbarton Bridge (Gostic 2018).

Stokes drift in the decomposition of Dyer (1974) is due to propagation of the tidal wave and is not expected to vary significantly on interannual timescales. Stokes drift at Dumbarton Bridge is expected to be net landward from the propagation of a standing wave down the axis of South Bay (Walters et al. 1985).

Methods

Suspended-sediment Flux Computation

Methods for the estimation of cross-section averaged suspended-sediment flux from WY 2009 to 2016 for the study location at Dumbarton Bridge (USGS station ID 373015122071000; Fig. 1) are presented in Part I, (Livsey et al. 2020). Livsey et al. (2020) modified methods for estimating suspended-sediment flux used by Shellenbarger et al. (2013) and references therein to account for changes in the vertical distribution of suspended sediment through the tide cycle. Accounting for changes in the vertical distribution of suspended sediment through the tide cycle reversed the sign of sediment flux estimates from net seaward flux (i.e., net flux out of LSB) to net landward flux (i.e., net flux into LSB) from WY 2009 to 2011.

Briefly, cross-section averaged sediment flux is estimated by regressing discrete measurements of cross-section SSC, water velocity, and area to continuous, 15-min, point-estimates of SSC and measurements of water velocity and stage measured at-a-point in the cross-section. Continuous SSC estimates are based on measurements from two optical turbidity sensors in the water column (mid-depth at 4 m below mean water depth and near-bed at 14 m below mean water depth; mean water depth is 15 m). Continuous water velocity and stage measurements are collected from a side looking ADCP. Cross-section averaged measurements of SSC are collected using an US-D96 sampler (Edwards et al. 1999). Cross-section averaged measurements of water velocity and area are collected using boat-based ADCP transects. Net suspended-sediment flux estimates are computed as the sum of the product of cross-section averaged time series of SSC and discharge (Livsey at al. 2020). Uncertainty in sediment flux estimates arising from scatter in regression equations was quantified using bootstrap and Monte-Carlo resampling described in Rustomji and Wilkinson (2008).

Suspended-sediment Flux Decomposition and Semidiurnal Variability

To determine the dominant components of the cross-section averaged suspended-sediment flux at Dumbarton Bridge suspended-sediment flux was decomposed following Dyer (1974) with

$$[Q_s] = [U][A][\mathrm{SSC}]\ (1) + [U'[A][\mathrm{SSC}]]\ (2) + [[U]A'[\mathrm{SSC}]]\ (3) + [U'A'][\mathrm{SSC}]\ (4) + [[U][A]\mathrm{SSC}']\ (5) + [U'[A]\mathrm{SSC}']\ (6) + [[U]A'\mathrm{SSC}']\ (7) + [U'A'\mathrm{SSC}']\ (8) \quad (1)$$

where brackets ([ ]) indicate tidally averaged values and prime (′) indicates deviations of instantaneous values from the tidal average (fluctuations). U and SSC are cross-section averaged water velocity and suspended-sediment concentration, respectively, and A is the cross-section area. As an example, for U, the decomposition takes the form

$$U = [U] + U' \quad (2)$$

in which U is the instantaneous value, $[U]$ is the tidally averaged value, and U' is the deviation from tidal average (fluctuation). Tidal averaging was performed using a low-pass Butterworth filter with a 30-h stop period and a 40-h pass period, a process that retains variations with periods longer than 30 h such as the spring-neap cycle. The filter was applied in the forward and reverse direction following Ganju and Schoellhamer (2006) to prevent filter-ringing anomalies at the beginning and end of time series. Terms 1, 4, and 6 are the fluxes due to the advective, Stokes drift due to the tidal wave propagation, and tidal dispersion processes, respectively. Hereafter, sediment flux owing to the advective process in term 1 will be referred to as "advective flux" and sediment flux owing to tidal dispersion in term 6 will be referred to as "dispersive flux." Further decomposition of terms that vary across the cross-section (e.g., Lerczak et al. 2006) is not possible because the index-velocity method (Ruhl and Simpson 2005; Levesque and Oberg 2012) and velocity-weighted cross-sectional average SSC measurements (Edwards et al. 1999) do not provide continuous cross-channel estimates of U, A, or SSC.

Semidiurnal variability of the advective flux and dispersive flux components was investigated by plotting the interquartile range of $[U][A]$, $U'[A]$, [SSC], SSC, and SSC' as a function of water velocity and inundated shoal area binned by tidal phase. Tidal phase was determined from times series of U. Sample time (t_i) was converted to tidal phase (θ_i) following Downing-Kunz and Schoellhamer (2013) with

$$\theta_i = \frac{t_i - t_{s1}}{t_{s2} - t_{s1}} * 360 \quad (3)$$

where t_{s1} is slack after flood (0°) and t_{s2} is the subsequent slack after flood (360°). Ebb tides occur between 0° and approximately 180°. The inundated area and volume south and north of Dumbarton Bridge were computed using stage measured at Dumbarton Bridge, tidal datums estimated from NOAA (2019), and computations of surface area using ArcGIS® (any use of trade, firm, or product names is for descriptive purposes only and does not imply endorsement by the U.S. Government) and bathymetry data from Fregoso et al. (2017). During ebb tides the inundated area south of Dumbarton Bridge was utilized. During flood tides the inundated area of South Bay between Dumbarton Bridge and 14 km north of the Dumbarton Bridge (i.e., the maximum tidal excursion estimated from U) was utilized. To delineate area and volume estimates between the main tidal channel and the shoals the − 6-m contour, identified by a change in slope between the shoals and channel, was utilized (Fig. 1).

Variability and Controls of Monthly and Annual Suspended-sediment Flux

Changes in net sediment flux at monthly and annual timescales were investigated to ascertain if changes in seasonal and/or annual sediment flux occurred from 2009 to 2011 into the 2013–2016 drought. Annual sediment fluxes for WY 2013 were omitted because sediment flux data are lacking from October 2012 to February 2013. Monthly and interannual variabilities in freshwater inflow, $\delta\rho/\delta x$, wind speed, and local tributary sediment fluxes were compared with net sediment flux estimates to investigate possible drivers of seasonal and interannual variabilities in sediment flux at Dumbarton Bridge (see Table 1 for details of data sources utilized). Freshwater inflow and changes in $\delta\rho/\delta x$ and $\delta\rho/\delta y$ are expected to affect advective fluxes through changes in along-channel and cross-channel exchange flow. Changes in wind-wave resuspension and local tributary sediment fluxes are expected to affect tidal dispersion by affecting $\delta\mathrm{SSC}/\delta x$ and $\delta\mathrm{SSC}/\delta y$.

$\delta\rho/\delta x$ were computed from continuous specific conductance and water temperature from three USGS monitoring locations between Central Bay and LSB (seaward (north) to landward (south): Alcatraz Island, San Mateo Bridge, and Dumbarton Bridge; Fig.1; Table 1). Water density was computed from specific conductance and water temperature using the method of Hill et al. (1986). Density time series were tidally filtered in the same manner presented earlier and utilized to compute $\delta\rho/\delta x$ between stations. Negative $\delta\rho/\delta x$ are expected to enhance landward along-channel exchange flow and net landward advective flux (Gostic 2018).

Direct analysis of $\delta\rho/\delta y$ is not possible because no long-term monitoring stations are located on the shoals. To provide an initial approximation of changes in $\delta\rho/\delta y$ we utilize salinity as a conservative tracer in a two-end member mixing model with

$$S_m = F_o S_O + F_R S_R \quad (4)$$

where S is salinity, S_m is measured salinity in the main tidal channel, and F is the fraction of water in South Bay from the specified source with "O" and "R" indicating water sources from the ocean and rivers, respectively. Assuming

Table 1 Data sources used in this study

Variable	Source
Freshwater inflow from the Delta	DAYFLOW, California Dept. of Water Resources (1986)
Freshwater inflow from LSB tributaries*	USGS, see footnote for site ID numbers**
Salinity and temperature data	USGS, see Fig. 1 for site locations and ID numbers
LSB tributary sediment flux*	Estimated using methods of Mckee et al. (2013) and gauged tributaries**
Wind speed and direction	NOAA, Redwood City site ID 9414523

*Minimum estimate, listed tributaries drain approximately 75% of the drainage area within one tidal excursion of Dumbarton Bridge

**All U.S. Geological Survey gaging data are available in the U.S. Geological Survey National Water Information System (NWIS; U.S. Geological Survey 2020): Guadalupe River (USGS Station ID: 11169025), Coyote Creek (USGS Station ID: 11172175), San Francisquito Creek (USGS Station ID: 11164500), Alameda Creek (USGS Station ID: 11179000), and Dry Creek (USGS Station ID: 11180500)

conservation of mass (i.e., $F_o + F_R = 1$), the fraction of freshwater in South Bay (F_R) can be estimated using

$$F_R = 1 - \frac{S_m - S_R}{S_O - S_R} \quad (5)$$

where 35 ppt and 0.5 ppt are utilized for S_O and S_R, respectively. Tidally filtered timeseries of salinity at Dumbarton Bridge and San Mateo Bridge are utilized for S_m. Estimates of F_R are compared with three-dimensional hydrodynamic estimates of van Kempen (2017) for WY 2015 and WY 2017. Based on past field-based and modeling studies (Powell et al. 1989; Pubben 2017; van Kempen 2017), F_R is expected to initially enhance positive $\delta\rho/\delta y$; however, for large values of F_R ($F_R > 0.5$), $\delta\rho/\delta y$ may become negative as saline water on the shoals is replaced by freshwater dispersed from the main tidal channel (Powell et al. 1989). Positive $\delta\rho/\delta y$ is expected to enhance shoal-to-channel sediment flux, while negative $\delta\rho/\delta y$ is expected to counteract, and even prevent, shoal-to-channel sediment flux (Lacy et al. 2014).

Because Schoellhamer (1996) and Lacy et al. (2014) found that increased northerly wind stress results in more resuspension on South Bay shoals and increased shoal-to-channel sediment flux per unit change in $\delta\rho/\delta y$ (Lacy et al. 2014) a multivariate regression with F_R and northerly wind stress to predict monthly sediment flux was included in the analysis of the effect of $\delta\rho/\delta y$ on monthly sediment flux. Wind stress (τ_w) was computed using $\tau_w = C_D\,\rho_{\text{air}} W_s^2$, using air density $\rho_{\text{air}} = 1.22$ kg/m^3 and drag coefficient $C_D = 1.2 \times 10{-}3$ (Pond and Pickard 1983) with wind measurements from Table 1.

Results

Suspended-sediment Flux Decomposition

Advective, dispersive, and Stokes drift components describe the majority of observed $[Q_s]$ with a coefficient of determination (R^2) between the sum of the advective, dispersive, and Stokes drift components and $[Q_s]$ of 0.99. The correlations of advective, dispersive, and Stokes drift components with $[Q_s]$ individually are 0.07, 0.81, and 0.01, respectively. The importance of dispersive flux in $[Q_s]$ as measured by R^2 did not change from WY 2009 to 2011 and WY 2013 to 2016. For WY 2009–2011 and WY 2013–2016 the dispersive flux accounted for 83% of the net $[Q_s]$ at Dumbarton Bridge (Table 2). For WY 2009–2011 and WY 2013–2016 advective flux at Dumbarton Bridge was net seaward, while dispersive flux and flux owing to Stokes drift due tidal wave propagation were net landward (Table 2). On a year-to-year basis the net-seaward advective flux was nearly balanced by a net-landward sediment flux driven by Stokes drift (Table 2).

Semidiurnal Variability in Components of Suspended-sediment Flux

Tidal phase averaging of the water flux components of advective and dispersive flux (i.e., $[U][A]$ and $U'[A]$, respectively) indicates that the sign of median $[U][A]$ for all tidal phases is seaward-directed and the magnitude of $U'[A]$ exhibits a flood-ebb asymmetry. In WY 2009–2011 and WY 2013–2016 two-sample t tests indicate that the magnitude of $U'[A]$ is higher in early ebb (< 75°) than early flood (180 to 255°), but in later flood, after 255°, $U'[A]$ is higher compared with later ebb (80–175°). The sign of $[U][A]$ and the flood-ebb asymmetry in $U'[A]$ did not change from WY 2009–2011 to WY 2013–2016 and is likely driven by the bathymetry of the tidal inlet at Dumbarton Bridge. Although landward along-channel exchange flow is expected to induce a net-landward advective flux for much of the year (Gostic 2018), hydrodynamics at the tidal inlet induce a predominantly seaward-directed $[U][A]$ and drives net-seaward advective flux for all years (Table 2). The flood-ebb asymmetry in $U'[A]$ will influence net dispersive flux but the sign of net dispersive flux also depends on semidiurnal variability in SSC′ detailed below.

Table 2 Net sediment fluxes by water year at Dumbarton Bridge. Landward is positive with median quantile estimates shown. Tributary sediment flux estimates computed using the methods of Mckee et al. (2013)

Water year	Advective flux (kt)	Dispersive flux (kt)	Stokes drift (kt)	Sum of advective flux and Stokes drift (kt)	Sum of advective flux, stokes drift, and dispersive flux (kt)	Net [Q_s] (kt)**	Total tributary Q_s ***	Alameda Creek Q_s ****
2009	− 117	248	83	− 34	214	250	98	77
2010	− 113	203	106	− 7	196	240	284	229
2011	− 92	− 232	113	21	− 211	− 151	245	204
2013*	− 77	− 53	86	9	− 44	− 32	173	59
2014	− 97	490	127	30	519	552	11	4
2015	− 155	552	171	16	568	609	98	68
2016	− 121	250	108	− 14	236	279	44	30
Total	− 773	1457	793	21	1478	1747	952	670

*Partial water year, data collection began Mar 7, 2013

**Differs from net sediment fluxes by water year in Fig. 6 because net sediment fluxes by water year are computed as the sum of the product of cross-section averaged SSC and discharge while data affected by filter-ringing anomalies in [Q_s] are removed

***Includes suspended-sediment flux from all gauged tributaries discharging within one-tidal excursion of Dumbarton Bridge

****Suspended-sediment flux from Alameda Creek, USGS station ID: 11179000

The interquartile range of [SSC] was nearly constant across tidal phase with the mean of median [SSC] across tidal phase increasing from 75 mg/l (±1.3 mg/l at 2 standard deviations) in WY 2009–2011 to 110 mg/l (±1.8 mg/l at 2 standard deviations) in WY 2013–2013. SSC and SSC′ covaried with water velocity and inundated shoal area (Fig. 2). Tidal phase averaging of SSC and SSC′ indicates relatively clear ebb waters (i.e., SSC′ < 0 and [U] < 0) from 0 to approximately 90° with an increase to turbid ebb waters (i.e., SSC′ > 0 and [U] < 0) after peak ebb velocity and when the inundated area of LSB is at a minimum (Fig. 2). On flood tides, SSC and SSC′ increase with peak flood velocity and when the rate of increase in the inundated area north of Dumbarton Bridge decreases (Fig. 2).

Larger SSC and SSC′ at the end of ebb tide (Fig. 2) is consistent with LSB shoals draining faster and more completely than South Bay shoals within 14 km north of Dumbarton Bridge. At mean lower low water, LSB shoals only retain 9% of the total inundated volume at mean higher high water compared with the 19% of the total inundated volume at mean higher high water on South Bay Shoals. At mean tide level, mean water depth on LSB shoals is 1.4 m and mean water depth on South Bay shoals is 2.0 m. For LSB at mean tide level, shoal volume accounts for 77% of the inundated embayment volume (i.e., main tidal channel plus shoals), while South Bay shoals account for 50% of the inundated embayment volume. At mean tide level for LSB and South Bay shoals combined, shoal volume accounts for 56% of the total inundated volume. The above volumetric calculations are consistent with past bathymetric analysis (Bearman et al. 2010) that indicted LSB shoals are shallower and narrower in profile than shoals in South Bay (Fig. 1).

From WY 2009 to 2011 and WY 2013 to 2016 the interquartile range of SSC increased from 32–150 mg/l in WY 2009–2011 to 54–165 mg/l in WY 2013–2016 and the interquartile range of SSC′ increased from − 36–160 mg/l in WY 2009–2011 to − 45–170 mg/l in WY 2013–2016 (Fig. 2). The increase in tidal phase averaged SSC from WY 2009–2011 to WY 2013–2016 is also seen in point SSC data from the mid-depth sensor at Dumbarton Bridge with increases in point SSC to pre-1999 levels when SSC were higher in the SFE overall (Fig. 3; Schoellhamer 2011). Two-sample t tests indicate the increase in SSC from WY 2009–2011 to WY 2013–2016 for all tidal phases was statistically significant (p < 0.05). Two-sample t tests indicate that changes in SSC′ from WY 2009–2011 to WY 2013–2016 for all tidal phases except from 20–45°, 125–150°, and 280–290° were statistically significant (p < 0.05).

Monthly and Annual Variability in Suspended-sediment Flux

In general, sediment flux measured at Dumbarton Bridge exhibits a seasonal pattern of net-landward flux during the wet season (October–February), variable net flux in the spring months (March–June), and near-zero net sediment flux during the dry season (July–September) (Fig. 4). Cumulative sediment flux into LSB measured at Dumbarton Bridge over the periods WY 2009–2011 and WY 2013–2016 was 342 kt (114 kt/year) and 1502 kt (429 kt/year), respectively, with net-

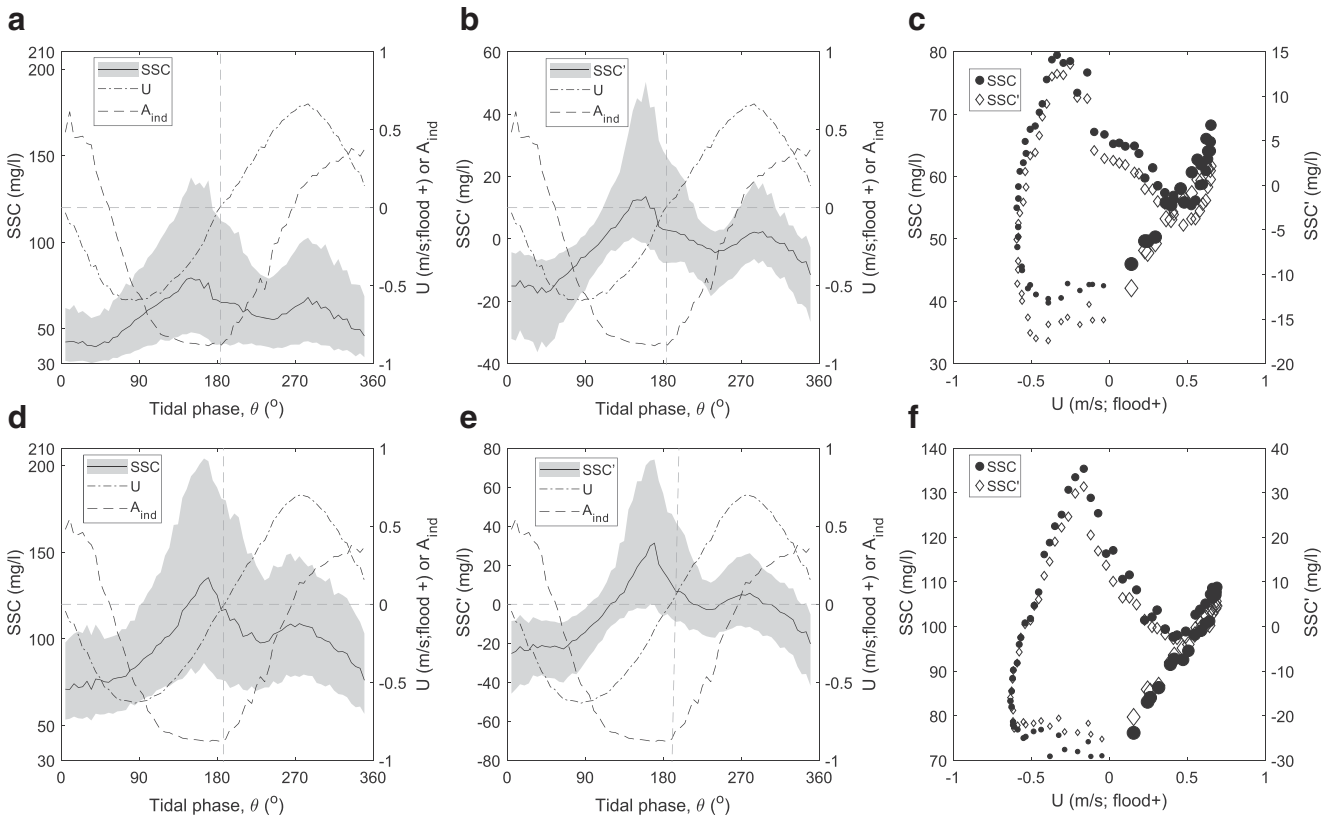

Fig. 2 Suspended-sediment concentration (SSC), deviation from tidally filtered SSC (SSC′), and cross-section averaged water velocity (U) plotted as a function of tidal phase for water year (WY) 2009–2011 (**a**, **b**, and **c**) and WY 2013–2016 (**d**, **e**, and, **f**). The inundated area (A_{ind}) south and north of Dumbarton Bridge for ebb (0 to approximately 180°) and flood tide (> 180 to 260°), respectively, is normalized to a mean of zero and a standard deviation of 1 for plotting purposes. Ebb tides end just after 180° due to tidal asymmetries. Note that SSC and SSC′ increased in WY 2013–2016 but that the relationships between SSC and SSC′ with tidal phase and U (**c** and **f**) remain the same from WY 2009–2011 to WY 2013–2016

landward flux increasing for all months in WY 2013–2016 (Fig. 5). Landward sediment flux into LSB increased from 114 kt/year (95% confidence interval 77 − 162 kt/year; WY 2009–2011) to 508 kt/year (95% confidence interval 384–662

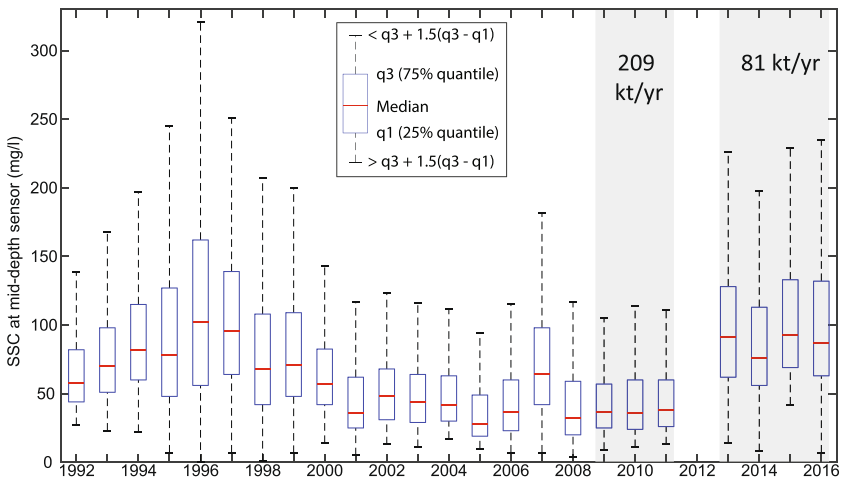

Fig. 3 Suspended-sediment concentration (SSC) at the mid-depth sensor at Dumbarton Bridge since water year (WY) 1992. Boxplots indicate median and interquartile range with outer lines to 1.5 times the interquartile range. Note median SSC during WY 2013–2016 has increased to pre-1999 levels. Estimates of mean annual tributary flux computed using the methods of Mckee et al. (2013) are indicated in grey shaded boxes for WY 2009–2011 and WY 2013–2016. Note that mean annual tributary fluxes decreased in WY 2013–WY 2016 while SSC increased

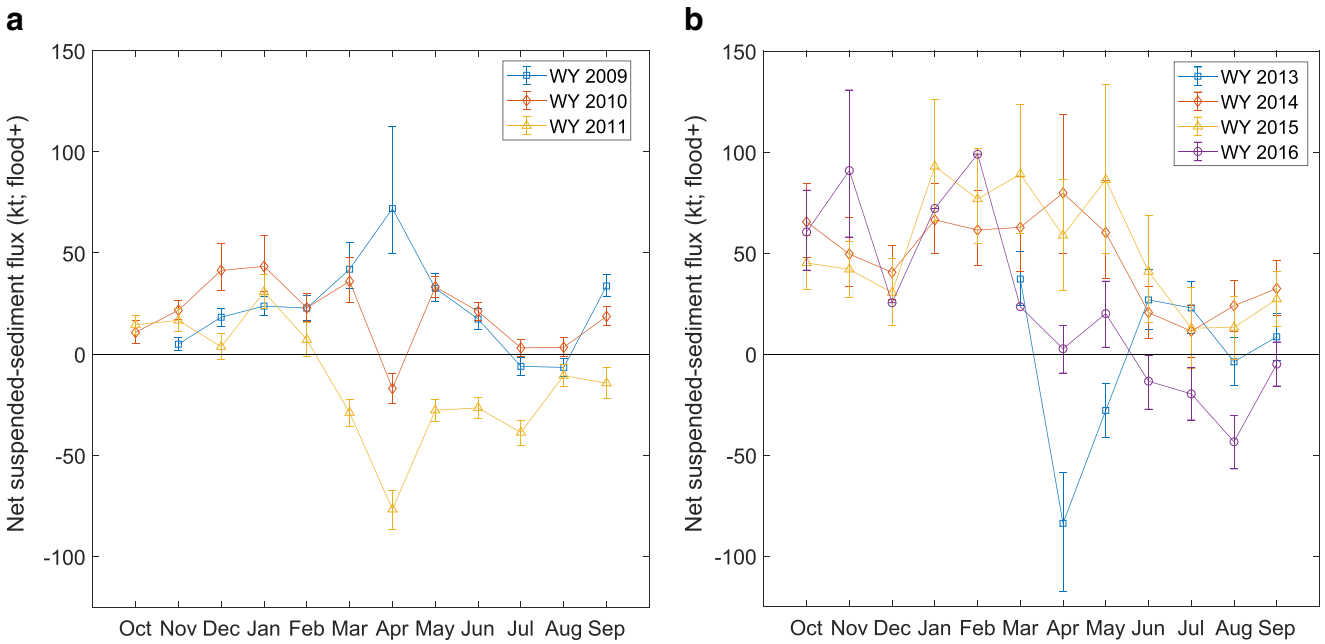

Fig. 4 Monthly net suspended-sediment flux computed at Dumbarton Bridge for **a** water year (WY) 2009–2011 and **b** WY 2013–2016. Error bars indicate 95% confidence intervals quantified using bootstrap and Monte-Carlo resampling described in Rustomji and Wilkinson (2008)

kt/year; WY 2014–2016 with WY 2013 omitted due to a lack of data from October 2012 to February 2013). Sediment flux from tributaries decreased in WY 2013 from 209 kt/year in WY 2009–2011 to 51 kt/year in WY 2014–2016 (Table 2). For all years except WY 2013 and WY 2014 sediment flux from Alameda Creek, seaward of Dumbarton Bridge (Fig. 1), accounted for the majority of tributary sediment flux (Table 2).

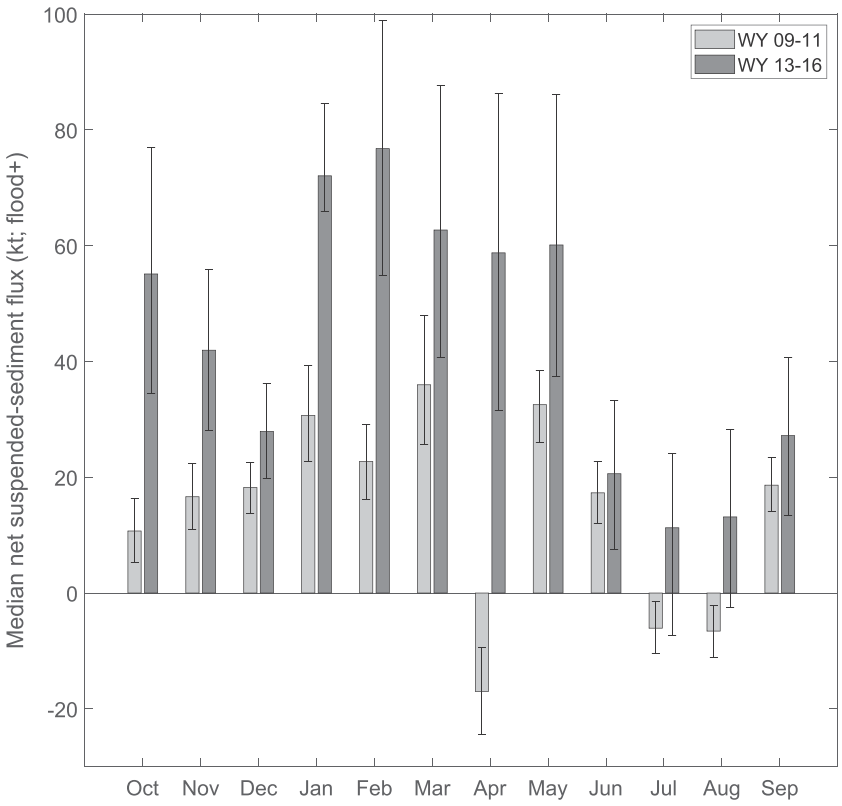

Fig. 5 Median monthly net suspended-sediment flux for water year (WY) 2009–2011 and WY 2013–2016 with 95% confidence intervals. Note WY 2013–2016 sediment flux into Lower South Bay (i.e., net-landward sediment flux) increased for all months relative to WY 2009–2011. About 95% confidence intervals were quantified using bootstrap and Monte-Carlo resampling described in Rustomji and Wilkinson (2008)

Controls on Annual and Monthly Suspended-sediment Flux–Freshwater Inflow, Along-channel and Cross-channel Density Gradients, and Wind

Freshwater inflow from LSB tributaries exhibited no statistically significant correlation with monthly sediment flux (R^2 = 0.03, p = 0.13). Freshwater inflow from the Delta exhibited a statistically significant correlation with monthly sediment flux (R^2 = 0.14, $p < 0.001$) with increases in freshwater inflow correlating with decreased sediment flux into LSB. On annual timescales, freshwater inflow from LSB tributaries and from the Delta exhibited statistically significant correlation with annual sediment flux estimates with increases in freshwater inflow correlating with decreased landward sediment flux into LSB (Fig. 6). Freshwater inflow from LSB tributaries and the Delta was greater in WY 2009–2011 compared with WY 2014–2016 for all years except WY 2016.

From November to April as freshwater inflow from the Delta and local tributaries increases, the magnitude of negative $\delta\rho/\delta x$ increases, while F_R increases (Figs. 7a, b, 8a, b). Median monthly $\delta\rho/\delta x$ and F_R are inversely proportional for all months (R^2 = 0.4, $p < 0.05$), possibly indicating that as landward along-channel exchange flow strengthens, channelward cross-channel flow weakens. For each WY, at the onset for freshwater inflow from the Delta, during the rising limb of the hydrograph, positive $\delta\rho/\delta x$ develops but the inversion in typical density gradients persisted for less than 3 weeks (Fig. 7). Consistent with past estimates of residence time (Walters et al. 1985) and hydrodynamic modeling results from van Kempen (2017), $\delta\rho/\delta x$ and F_R change faster in the wet season compared with the dry season.

Annual maxima in F_R are in close agreement with hydrodynamic modeling estimates of peak F_R in WY 2015 and 2017 (Fig. 9a). The annual maxima in F_R is proportional to total annual freshwater inflow from the Delta (Fig. 9a) and net annual LSB sediment flux (Fig. 9b). When peak annual F_R exceeds 0.56, that is when freshwater accounts for more than 56% of the volume of water in the main tidal channel, net annual LSB sediment flux goes from net-landward to net-seaward (Fig. 9b). Note that 56% is the estimated volume of LSB and South Bay shoals at mean tide level. Annual maxima in F_R is expected to be an important indicator of $\delta\rho/\delta y$ because the replacement of freshwater in South Bay with ocean-derived water takes many months (Fig. 7; van Kempen 2017).

Median monthly $\delta\rho/\delta x$ measured between Dumbarton Bridge and Alcatraz Island, Dumbarton Bridge and San Mateo Bridge, and San Mateo Bridge and Alcatraz Island regressed to monthly sediment flux for all months except from July to November in WY 2014–2016 indicate decreased landward sediment flux into LSB with more negative density

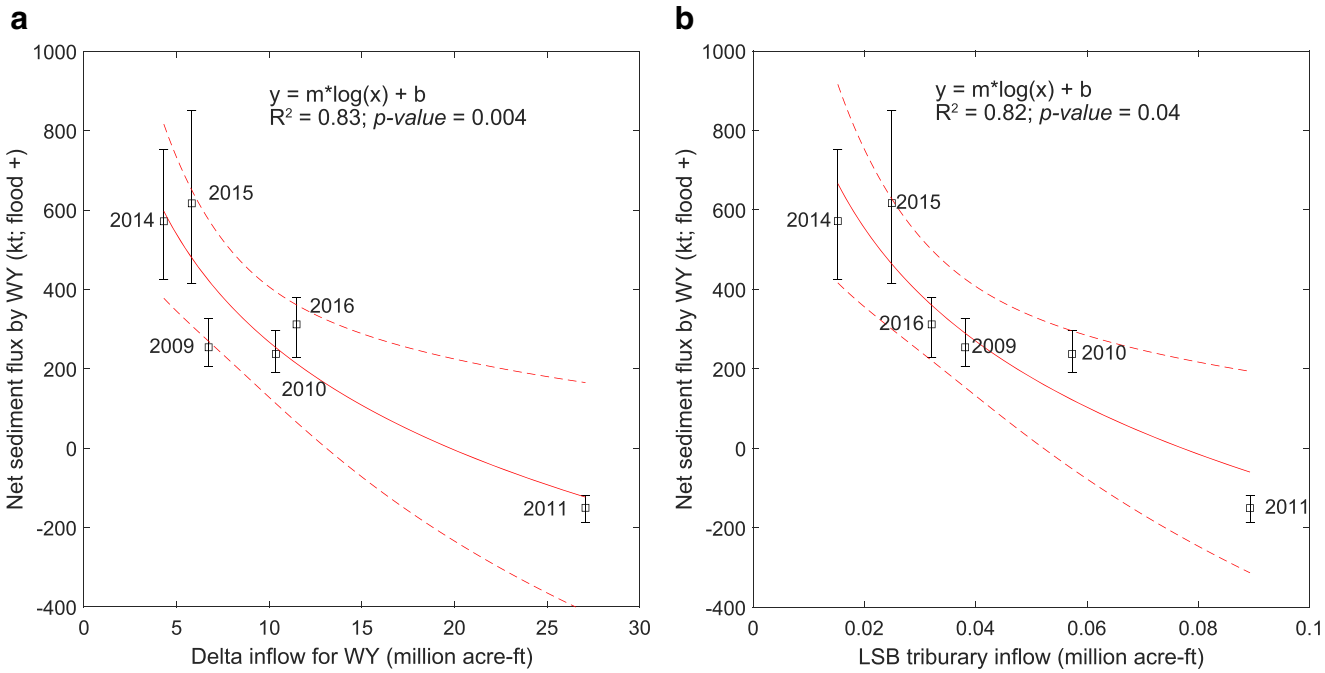

Fig. 6 Annual freshwater inflow from the Sacramento San-Joaquin Delta (Delta) (**a**) and LSB tributaries by water year (WY) (**b**) regressed to net-annual suspended-sediment flux at Dumbarton Bridge. Log-linear models provided best fit for freshwater inflow from the Delta (**a**) and Lower South Bay (LSB) tributaries (**b**) regressed to water year cumulative sediment flux. Confidence intervals were quantified using bootstrap and Monte-Carlo resampling described in Rustomji and Wilkinson (2008). Optimum functional forms for regression were selected using the regression diagnostics of Helsel and Hirsch (2002). Dashed, red lines indicate 95% prediction confidence intervals. A log-linear model was expected because freshwater inflow from the Delta exhibits log-linear relationship with salinity throughout the San Francisco Estuary (Shellenbarger and Schoellhamer 2011), and freshwater inflow from the Delta is expected to affect sediment flux at Dumbarton Bridge through changes in density gradients that affect along-channel and cross-channel exchange flow

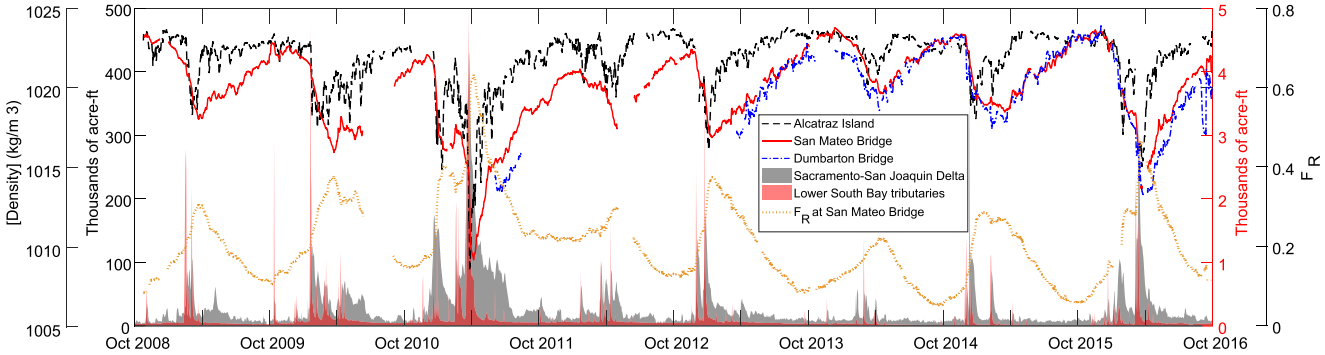

Fig. 7 Time series of tidally filtered water density at Dumbarton Bridge, San Mateo Bridge, and Alcatraz Island, freshwater inflow volume from the Sacramento-San Joaquin Delta and Lower South Bay tributaries, and F_R computed from tidally filtered salinity at the upper sensor at San Mateo Bridge. At Dumbarton Bridge and San Mateo Bridge two sensor elevations are occupied, only data from the upper sensors at Dumbarton Bridge and San Mateo Bridge are shown as data from the lower sensors plot near data from the upper sensors. Salinity and temperature monitoring at Dumbarton Bridge was intermittent in water year (WY) 2009–2011. Note that at the onset of freshwater inflow from the Delta, that is during the rising limb, negative (i.e., landward decreasing) density gradients weaken for 1 to 3 weeks but subsequently recover and strengthen during the falling limb. Only F_R from the upper sensor at San Mateo Bridge is shown because salinity monitoring at Dumbarton Bridge was intermittent in WY 2009–2011. F_R from Dumbarton Bridge and San Mateo Bridge exhibit very similar variability.

gradients ($R^2 \leq 0.2$, $p < 0.05$). Conversely, median monthly $\delta\rho/\delta x$ defined between San Mateo Bridge and Dumbarton Bridge analyzed from July to November in WY 2014–2016 indicate increased landward sediment flux into LSB with more negative $\delta\rho/\delta x$ ($R^2 = 0.5$, $p < 0.02$). $\delta\rho/\delta x$ from July to November in WY 2014–2016 was analyzed separately because density at San Mateo Bridge exceeded density at Alcatraz Island in WY 2014–2016, and wet season freshwater inflow was delayed until early December in these years (Fig. 7). When density at San Mateo Bridge exceeds density at Alcatraz Island and Dumbarton Bridge, landward along-channel exchange flow and net-landward sediment flux are expected landward of San Mateo Bridge, while seaward along-channel exchange flow is expected seaward of San Mateo Bridge (Largier et al. 1997).

Maximum monthly F_R estimated at Dumbarton Bridge and San Mateo Bridge for all months indicates decreased net-landward sediment flux with increasing F_R ($R^2 \leq 0.1$, $p < 0.01$). The sign of the regression between maximum monthly F_R and monthly sediment flux did not change from July to November in WY 2014–2016. Maximum monthly F_R was used to estimate the effect of $\delta\rho/\delta y$ on sediment flux because shoal-to-channel sediment flux induced by positive $\delta\rho/\delta y$, and channelward cross-channel exchange flow is expected to be event driven (Lacy et al. 2014). Inclusion of mean northerly wind stress with maximum monthly F_R from either Dumbarton Bridge or San Mateo Bridge exhibited better correlation ($R^2 \leq 0.3$, $p < 0.001$) with monthly sediment flux than use of F_R alone. Maximum monthly F_R and mean northerly wind stress were both statistically significant variables in the multivariate regression ($p < 0.001$). Inclusion of monthly measures of $\delta\rho/\delta x$ did not improve model fit.

Median annual wind speed in WY 2009–2011 is 2.3 m/s, and median annual wind speed from WY 2013 to 2016 is 2.2 m/s. Wind speed analyzed on seasonal timescales (e.g., wet-season months, dry season months), and with respect to wind direction (e.g., trends in northerly or easterly wind speeds), indicate little to no change or possible decrease from WY 2009 to 2011 and WY 2013 to 2016 (Fig. 8c, d). Trends in wind speed from WY 2009–2011 to WY 2013–2016 are consistent with Bever et al. (2018) who documented an estuary-wide decrease in wind speed from 1995 to 2015.

Discussion

Controls on Lower South Bay Sediment Flux

Dispersive flux due to tidal dispersion was the dominant process of $[Q_s]$ and drove the increase in net-landward sediment flux into LSB in WY 2013–2016 (Table 2). Of the three components of dispersive flux, SSC′ was the only component to increase from WY 2009–2011 to WY 2013–2016. Timing of SSC′ with respect to tidal phase and water velocity was similar from WY 2009–2011 to WY 2013–2016 (Fig. 2). Tidal phase averaging of SSC′ indicates that net landward dispersive flux is driven by asymmetries in water level between slack after flood and slack after ebb tides. SSC and SSC′ throughout much of the flood tide is elevated with respect to the onset of ebb tide because resuspended shoal sediment seaward of Dumbarton Bridge has been concentrated into the channel on the previous ebb tide and because of increased wind-wave resuspension during low water after ebb tide (Lacy et al. 1996). Net landward sediment flux at Dumbarton Bridge is consistent with bathymetric analyses by Jaffe and Foxgrover (2006) and Bearman et al. (2010) that indicated that shoals north of Dumbarton Bridge were net erosional and shoals in LSB were net depositional from 1956 to 2005.

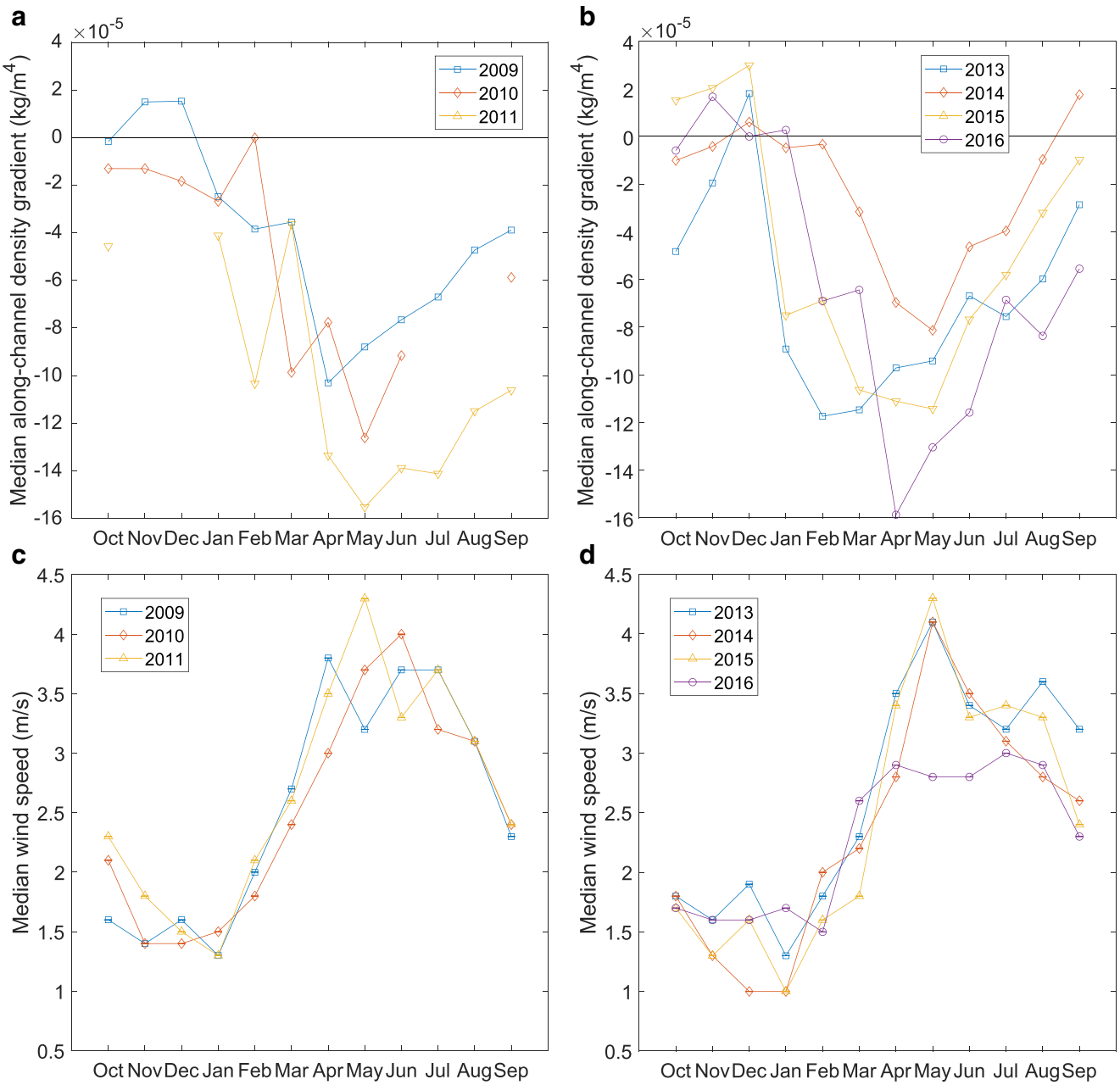

Fig. 8 **a**,**b** Monthly median along-channel density gradients by water year (WY) defined between the upper sensor at San Mateo Bridge and Alcatraz Island. Monthly median along-channel density gradients defined between Dumbarton Bridge and Alcatraz Island and Dumbarton Bridge and San Mateo Bridge exhibit the same seasonal pattern in along-channel density gradients shown. **c**,**d** Monthly median wind-speed measured at Redwood City, CA, by WY (NOAA Station 9414523; Fig. 1)

Net-landward dispersive flux is somewhat surprising because past studies (Schoellhammer 1996; Schoellhamer et al. 2007; Crauder et al. 2016) and current monitoring (Buchanan et al. 2018) all indicate SSC increases landward in South Bay. Analysis of $\delta SSC/\delta x$ at Dumbarton Bridge, estimated by fitting SSC over Lagrangian coordinates computed between slack tides, indicates that $\delta SSC/\delta x$ is positive (i.e., landward increasing) for 88% of the tides from WY 2009 to 2011 and WY 2013 to 2016. Increases in the availability of sediment in the main tidal channel on flood compared with ebb tide coupled with a flood-positive settling lag (Chernetsky et al. 2010) is thought to drive net-landward dispersive flux counter to the positive $\delta SSC/\delta x$. The flood-positive settling lag is driven by tidal inlet hydrodynamics that induce a flood-asymmetry in U' and enhanced by larger suspended-sediment settling velocity on flood tides (Livsey et al. 2020).

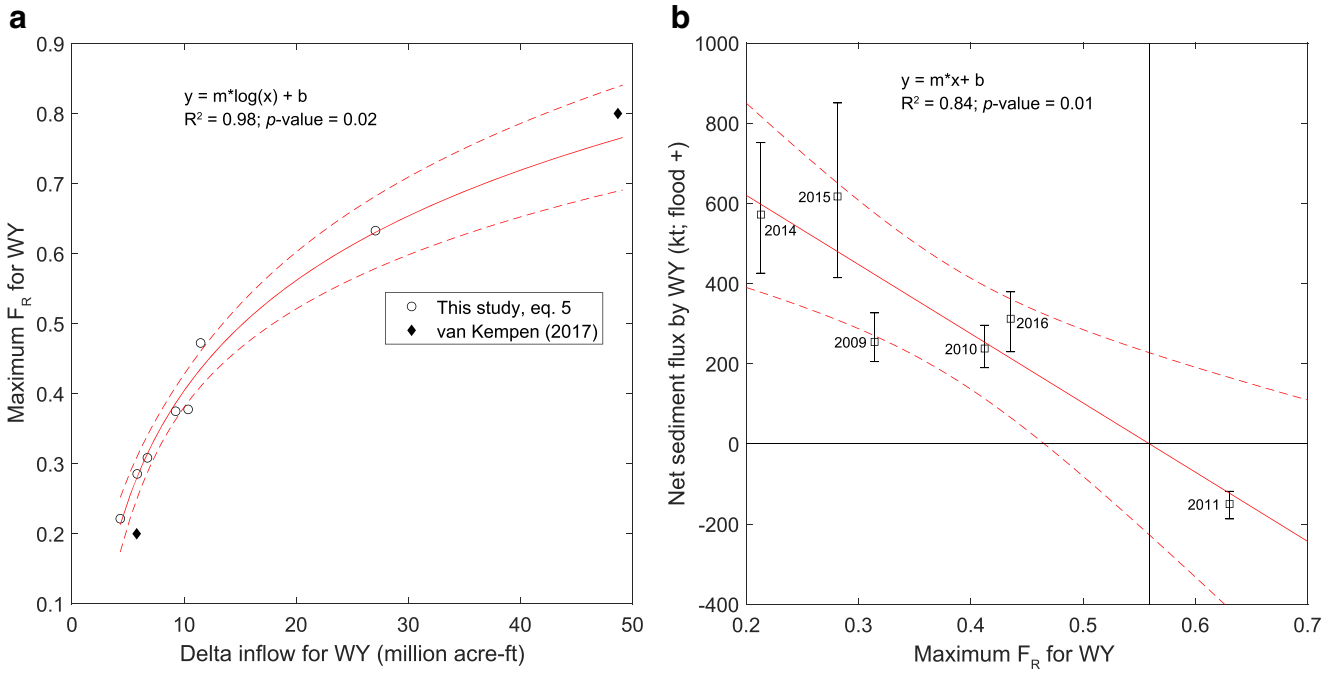

Fig. 9 **a** Comparison of maximum annual F_R at San Mateo Bridge to model results from van Kempen (2017). Salinity data from San Mateo Bridge was utilized to estimate F_R because salinity monitoring at Dumbarton Bridge was intermittent in water year (WY) 2009–2011. The regression shown only utilized F_R estimates from this study. Dashed, red lines indicate 95% prediction confidence intervals. A log-linear model was expected because freshwater inflow from the Sacramento San-Joaquin Delta (Delta) exhibits log-linear relationship with salinity throughout the San Francisco Estuary (Shellenbarger and Schoellhamer 2011). **b** Maximum annual F_R at San Mateo Bridge compared with net-annual suspended-sediment flux at Dumbarton Bridge. Dashed, red lines indicate 95% prediction confidence intervals of linear regression

Conceptual Model of Lower South Bay Sediment Flux

The increase in SSC, SSC′, and landward dispersive flux that drove increased landward sediment flux at Dumbarton Bridge in WY 2013–2016 was likely not from increases in wind speed and tributary fluxes because wind speed decreased in South Bay from 1995 to 2015 (Bever et al. 2018) and tributary fluxes decreased in WY 2014–2016 (Table 2). An increase in shoal-sediment erodibility is not expected to have driven the increase in SSC and SSC′ because no mechanism is known to increase shoal sediment erodibility during all months (Fig. 5).

The increase in SSC, SSC′, and landward dispersive flux is hypothesized to be driven by (1) enhanced shoal-to-channel sediment flux caused by decreased freshwater inflow from the Delta that enhanced positive $\delta\rho/\delta y$ and channelward cross-channel exchange flow and (2) increased convergence of South Bay sediment landward of San Mateo Bridge in the dry season. Enhanced shoal-to-channel sediment flux and convergence of sediment landward of San Mateo Bridge increases the availability of sediment in the main tidal channel whereupon the flood-asymmetry in water velocity drives net-landward dispersive flux.

Conceptually, during wet years (maximum annual $F_R >$ 0.56; Fig. 9b), the volume of freshwater entering South Bay is sufficient to replace saline water on the shoals, thus reducing or inverting positive $\delta\rho/\delta y$ (e.g., McCulloch et al. 1970; Powell et al. 1989; Huzzey et al. 1990) and decreasing shoal-to-channel sediment flux (Lacy et al. 2014). During dry years (maximum annual $F_R < 0.56$; Fig. 9b), freshwater is more confined to the main tidal channel and salinity on the shoals remains elevated, thus increasing the positive shoal-to-channel $\delta\rho/\delta y$ (e.g., McCulloch et al. 1970; Powell et al. 1989; Huzzey et al. 1990) and increasing the shoal-to-channel sediment flux (Lacy et al. 2014). In addition, in WY 2014–2016 density at San Mateo Bridge exceeded density at Alcatraz Island in summer months (Fig. 7). Landward along-channel exchange flow, between San Mateo Bridge and LSB during these conditions, counteracts net-seaward wind-driven advective flux in the main channel and is thought to induce convergence of sediment south of San Mateo Bridge (Largier et al. 1997). Below we expand the above hypothesis to a conceptual model that further explains seasonal changes in LSB sediment flux between the dry season (July–September; Fig 10a), wet season (October–February; Fig 10b), and spring (March–June; Fig. 10c, d).

During the dry season the magnitude of negative $\delta\rho/\delta x$ and positive $\delta\rho/\delta y$, induced by freshwater inflow during the preceding wet season, approaches zero (Fig. 10a) (Figs. 8a, c, 10a; Powell et al. 1989; Lacy et al. 2014). Landward along-channel exchange flow is at a minimum, while persistent diurnal winds (Fig. 8c, d) from the northwest induce barotropic circulation that drives net-landward advective flux over the

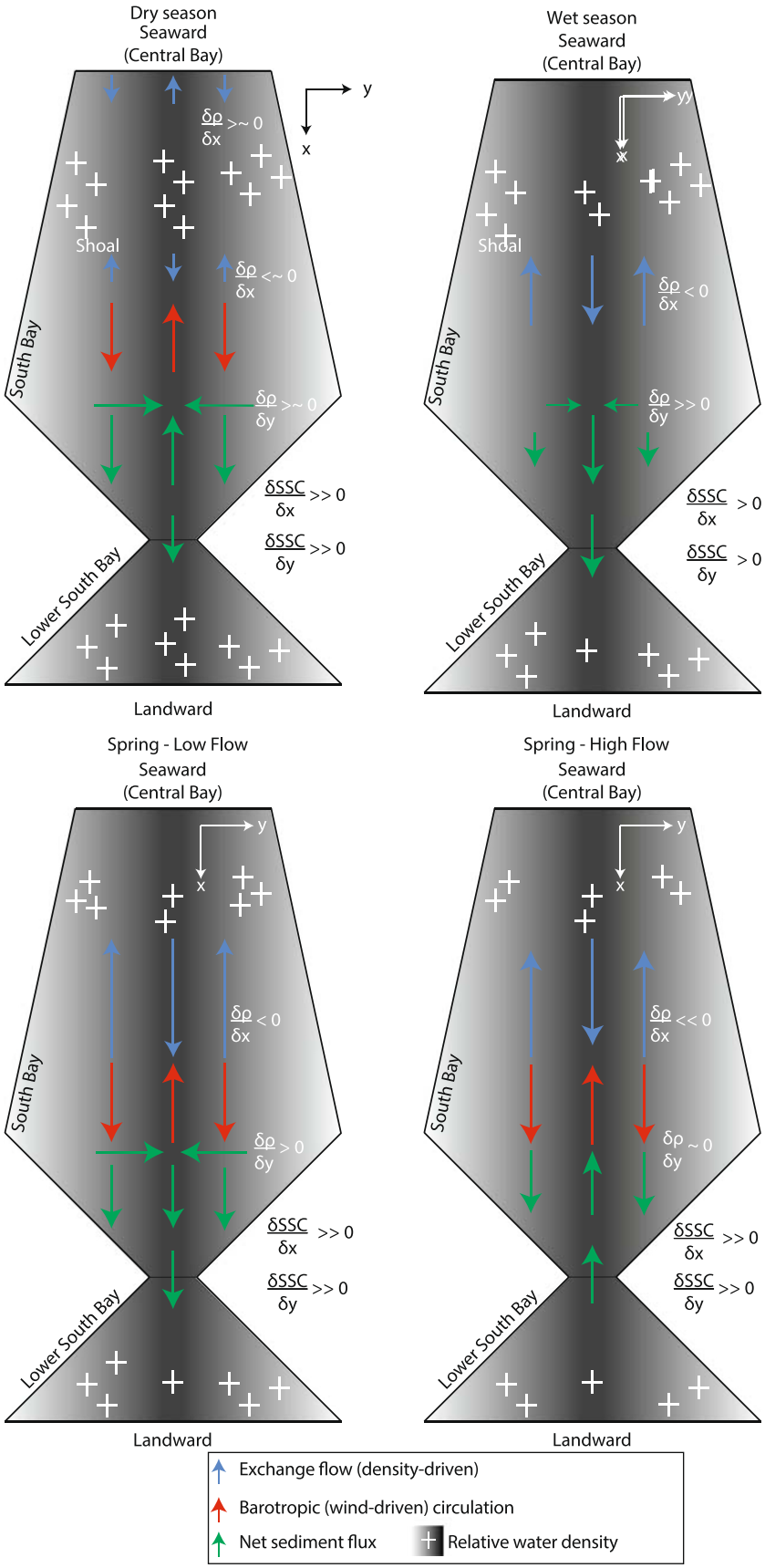
Dry season
Seaward
(Central Bay)
y
x
δρ/δx >~ 0
Shoal
δρ/δx <~ 0
South Bay
δρ/δy >~ 0
δSSC/δx >> 0
δSSC/δy >> 0
Lower South Bay
Landward
Wet season
Seaward
(Central Bay)
yy
xx
Shoal
δρ/δx < 0
South Bay
δρ/δy >> 0
δSSC/δx > 0
δSSC/δy > 0
Lower South Bay
Landward
Spring - Low Flow
Seaward
(Central Bay)
y
x
δρ/δx < 0
South Bay
δρ/δy > 0
δSSC/δx >> 0
δSSC/δy >> 0
Lower South Bay
Landward
Spring - High Flow
Seaward
(Central Bay)
y
x
δρ/δx << 0
South Bay
δρ/δy ~ 0
δSSC/δx >> 0
δSSC/δy >> 0
Lower South Bay
Landward
Exchange flow (density-driven)
Barotropic (wind-driven) circulation
Net sediment flux
Relative water density

◀ **Fig. 10** Conceptual model of South Bay and Lower South Bay suspended-sediment flux in the dry season (**a**; July–September), wet season (**b**; October–February), and spring (**c,d**; March–June). Along-channel (x, landward positive) and cross-channel (y, landward positive) density gradients are denoted by $\delta\rho/\delta x$ and $\delta\rho/\delta y$, respectively. δSSC/δx is the along-channel SSC gradient at Dumbarton Bridge. δSSC/δy is the cross-channel SSC gradient from the main tidal channel to the shoals. $\delta\rho/\delta x$ in all panels except panel **a** is defined between Lower South Bay and Central Bay. In the dry season (**a**), salinity in South Bay may exceed salinity in Lower South Bay and Central Bay (e.g., Fig. 7), resulting in negative $\delta\rho/\delta x$ landward of the more saline region in South Bay, and positive $\delta\rho/\delta x$ seaward of the more saline region. The length of arrows indicates the magnitude of the along-channel exchange flow (blue arrows), baroclinic circulation (red arrows), and net sediment flux (green arrows). The number of white "plus signs" indicates relative salinity

shoals and net-seaward advective flux in the main channel (Lacy et al. 2014). During dry years, net-landward advective flux in the main channel may be increased when salinity in South Bay exceeds LSB and Central Bay salinity (i.e., negative $\delta\rho/\delta x$ from South Bay to LSB but positive $\delta\rho/\delta x$ from Central Bay to South Bay; Fig. 7) and a landward along-channel exchange flow between South Bay and LSB counteracts barotropic circulation (Fig. 10a; Largier et al. 1997). Net sediment flux from the shoals to the channel is enhanced when positive $\delta\rho/\delta y$ and channelward cross-channel exchange flow develops from wind-induced cooling of shoal water and/or increased wind-wave suspension on the shoals driving increased-positive δSSC/δy (Lacy et al. 2014).

Although positive $\delta\rho/\delta y$ in the dry season are less than the wet season, enhanced wind wave resuspension drives more positive δSSC/δy and thereby enhanced shoal-to-channel sediment flux (Figs. 10a; 9b, Lacy et al. 2014). Net-landward dispersive flux at Dumbarton Bridge occurs due to increased availability of sediment in the main tidal channel; however, net-seaward barotropic flow in the main tidal channel may reduce net-landward dispersive flux in the dry season by advection of shoal-derived sediment in the main tidal channel seaward from LSB (Fig. 10a). The seasonal reduction of net-landward sediment flux at Dumbarton Bridge in the dry season (Fig. 4) is thought to be from reduced shoal-to-channel fluxes as freshwater in the main-tidal channel is replaced by saline ocean-derived water (Fig. 7), and positive $\delta\rho/\delta y$, developed during preceding wet season, decrease. Deposition of sediment on the shoals is expected to increase later in the dry season as diurnal winds persist but positive $\delta\rho/\delta y$ and shoal-to-channel fluxes decrease.

In the wet season, during the falling-limb of the hydrograph, freshwater inflow from the Delta induces more negative $\delta\rho/\delta x$ (Figs. 7, 8c, d), and conceptually, positive $\delta\rho/\delta y$ would reach an annual maximum (e.g., Lacy et al. 2014; Fig. 10b). With the onset of freshwater inflow from the Delta, $\delta\rho/\delta x$ can become positive and drive net-seaward sediment flux from LSB with the inversion in typical density gradients occurring on time-scales of days to a few weeks (Fig. 7; Gostic 2018). Reduced wind speeds (Fig. 8c, d) and variable wind direction result in negligible barotropic circulation (Brand et al. 2010; Lacy et al. 2014). Negative $\delta\rho/\delta x$ induces landward along-channel exchange flow in the channel and a net-seaward advective flux on the shoals; however, landward-directed dispersive flux from enhanced wind-wave suspension during low water is expected to maintain net-landward sediment flux on the shoals (Lacy et al. 1996). Positive $\delta\rho/\delta y$ is expected to reach an annual maximum because freshwater inflow from the Delta is preferentially dispersed along the main tidal-channel and salinity on the shoals has reached an annual maximum in the preceding dry season. Although positive $\delta\rho/\delta y$ are at an annual maximum, shoal-to-channel fluxes in the wet season are smaller than the dry season because of reduced wind wave resuspension and decreased positive δSSC/δy (Fig. 10b; Lacy et al. 2014). That said, increased net-landward sediment flux at Dumbarton Bridge compared with the dry season is expected because landward along-channel exchange is not counteracted by barotropic residual circulation.

In the spring months (March–May) the magnitude of negative $\delta\rho/\delta x$ is at a maximum (Fig. 8a, b) and landward exchange flow reaches an annual maximum (Fig. 10c, d), while $\delta\rho/\delta y$ depends on the volume of the wet-season freshwater inflow from the Delta (McCulloch et al. 1970; Powell et al. 1989). Springtime sediment flux at LSB is expected to be net-landward in dry years ($F_R < 0.56$;Fig. 10c) and net-seaward in wet years ($F_R > 0.56$; Fig. 10d). Increased wind-speeds in the spring months increase positive δSSC/δy but the sign of net dispersive flux is thought to be affected by $\delta\rho/\delta y$ that influences the supply of sediment in the main tidal channel seaward of Dumbarton Bridge. In spring of dry years (Fig. 10c), greater positive $\delta\rho/\delta y$ and increased shoal-to-channel fluxes are expected (Powell et al. 1989; Huzzey et al. 1990; Lacy et al. 2014). However, in spring of wet years (Fig. 10d), smaller positive or negative $\delta\rho/\delta y$ are expected (Powell et al. 1989; Huzzey et al. 1990; Lacy et al. 2014). In wet years with reduced positive and/or negative $\delta\rho/\delta y$, shoal-to-channel fluxes are reduced. Presumably, decreased positive $\delta\rho/\delta y$ would reduce shoal-to-channel flux in LSB as well; however, because shoals in LSB are narrower and shallower than shoals in South Bay, shoal-to-channel fluxes in LSB are expected to be less sensitive to changes in $\delta\rho/\delta y$ than shoals in South Bay. Reduced availability of sediment in the main tidal channel on flood tides allows the persistent positive δSSC/δx to drive net-seaward dispersive flux for several months (e.g., WY 2011 March to September; Fig 4a).

The above conceptual model explains why negative $\delta\rho/\delta x$ for most months is correlated with decreased landward sediment flux. $\delta\rho/\delta x$ is inversely related to $\delta\rho/\delta y$ but if the volume of freshwater inflow from the Delta is sufficient to replace the majority of South Bay water, positive $\delta\rho/\delta y$ will decrease and

may become negative. The model also provides an explanation why net-landward sediment flux increased in WY 2014–2016 by 345% when sediment flux from local tributaries declined by 75% (Table 2). We note that the onset of wet-season conditions, primarily determined by the onset of freshwater inflow from the Delta, varies by WY (e.g., WY 2014, Figs. 7, 8b). With the onset of freshwater inflow from the Delta delayed, and barotropic residual circulation at a minimum from October to February, net-landward advective flux in the main channel induced by salinity in South Bay exceeding salinity in Central Bay and LSB would enhance transport of sediment into LSB. The above analysis suggests that at least in dry years, the primary source of sediment to LSB is from South Bay shoals. Because the eastern shoal of South Bay is much broader than the western shoal (5–10 km versus 2–5 km; Fig. 1), the eastern shoal is expected to provide more sediment to LSB. In relatively wet years (e.g., WY 2010), sediment flux from Alameda Creek may be an important source of sediment to LSB as well (Fig. 1; Table 2). Additional monitoring and/or modeling of salinity, temperature, and SSC on the shoals of South Bay could be used to test the above conceptual model.

We focus the above discussion on freshwater inflow from the Delta because past studies indicate freshwater inflow from the Delta is the primary driver of $\delta\rho/\delta x$ and $\delta\rho/\delta y$ in the SFE (McCulloch et al. 1970; Shellenbarger and Schoellhamer 2011; Pubben 2017; Gostic 2018). Conceptually, freshwater inflow from LSB tributaries would have a similar, albeit smaller, influence on $\delta\rho/\delta x$ and $\delta\rho/\delta y$. However, note that freshwater from Alameda Creek could have a significant impact on $\delta\rho/\delta y$ as freshwater from the tributary discharges immediately onto the eastern shoal of Sough Bay (Fig. 1). Additional monitoring and modeling of water density on the eastern shoal of South Bay could elucidate if the correlation between freshwater inflow from LSB tributaries and annual sediment flux (Fig. 6) is causal or simply driven by the correlation between freshwater inflow from the Delta and LSB tributaries on monthly timescales ($R^2 = 0.69$; $p = 0.11$). That said, changes in timing, magnitude, and duration of freshwater inflow between LSB and South Bay tributaries and the Delta may be important to consider for other years.

Implications for Lower South Bay Tidal-marsh Restoration

Using net-annual sediment flux estimates, LSB basin-wide sediment accumulation rates can be estimated using a bulk density (617 kg/m^3; the mean bulk density of 7 cores collected in South Bay; Caffrey 1995; Love et al. 2003) and area of the basin (34 km^2 at mean tide level; Hager and Schemel 1996). For WY 2009, 2010, and 2011 basin-wide sediment accumulation rates were 12 ± 3 mm, 11 ± 3 mm, and − 7 ± 1 mm, respectively; with the negative value in 2011, the wettest year from WY 2009 to 2016, indicating erosion. For WY 2014, 2015, and 2016 basin-wide sediment accumulation rates were 28 ± 7 mm, 30 ± 11 mm, and 15 ± 4 mm, respectively. The average sediment flux and basin-wide sediment accumulation rate from WY 2009 to 2011 and WY 2014 to 2016 were 311 kt/year and 15 mm/year, respectively. An average basin-wide sediment accumulation rate of 15 mm/year from WY 2009 to 2011 and WY 2014 to 2016 is close to a previously published average accretion rate from 1983 to 2005 in LSB, based on bathymetric surveys, of 20 mm/year (Jaffe and Foxgrover 2006).

WY 2009–2010 and 2014–2015 basin-wide sediment accumulation rates are above measured mean sea level rise of 2.17 mm/year at the Golden Gate (Flick et al. 2003) suggesting that accretion can keep up with current rates of mean sea level rise. However, Cayan et al. (2008) projected a maximum sea level rise of 1.24 m in the SFE from 2000 to 2100 or a mean rate of 12.4 mm/year, near the basin-wide sediment accumulation rates observed during WY 2009–2011. Sediment flux into LSB is greater than previously computed by Shellenbarger et al. (2013), indicating that more sediment is available for stabilizing tidal channels, mudflat accretion, and marsh accretion and that tidal marshes of LSB may be more resilient to sea level rise than previously thought. That said, the response of tidal marshes to sea level rise is a complex interaction of hydrodynamics, geomorphology, ecology, and climate that should be evaluated locally (D'Alpaos et al. 2007; Fagherazzi et al. 2012; Kirwan et al. 2016).

If the increase in net-landward sediment flux at LSB from WY 2014 to 2016 was driven by increased shoal-to-channel fluxes in South Bay, less sediment may have been delivered to portions of the South Bay Salt Pond Restoration Project seaward of LSB (Fig. 1). Additional, contemporaneous monitoring of accretion and shoal-to-channel fluxes in South Bay and LSB could be used to ascertain how shoal-to-channel fluxes in South Bay and LSB interact and impact accretion throughout the South Bay Salt Pond Restoration Project.

Broader Implications

The linkage of LSB sediment flux to freshwater inflow from the Delta is consistent with past studies in the SFE (McCulloch et al. 1970; Conomos et al. 1985; Walters et al. 1985; Largier et al. 1997; Kimmerer 2002; Gostic 2018) and with circulation characteristics of "low-inflow" estuaries that are highly sensitive to changes in freshwater inflow (Largier et al. 1997; Schettini et al. 2017). The linkage of LSB sediment flux to freshwater inflow from the Delta (Figs. 6a, 9b) may indicate LSB sediment flux can be affected by changes in water use and/or changes in flow magnitude and timing from the Sierra Nevada expected this century (Knowles and Cayan 2002).

The proposed relationship between LSB sediment flux and the volume of freshwater inflow from the Delta is primarily

owing to the channel-shoal bathymetry of South Bay. For estuaries exhibiting channel-shoal bathymetry, a similar sensitivity of shoal-to-channel sediment flux to freshwater inflow volume may occur. The importance of $\delta\rho/\delta y$ on shoal-to-channel sediment flux is expected to increase as shoal width exceeds the cross-channel tidal excursion. Furthermore, because the cross-channel tidal excursion on shoals varies with shoal-depth, changes in the sensitivity of shoal-to-channel sediment flux to cross-channel density may result in convergence of sediment in some portions of the estuary and divergence of sediment in other portions.

Conclusions

Suspended-sediment flux at the boundary of a subembayment in San Francisco Estuary over 6 years is analyzed to understand controlling factors and investigate the impacts of the recent drought in California. During the recent drought in California from water year (WY) 2013 to WY 2016, transport of sediment into Lower South Bay, the southernmost subembayment of San Francisco Estuary, increased by 345% relative to WY 2009–2011 from 114 to 429 kt/year. This follows previous observations in Lower South Bay that found during wetter years sediment flux into Lower South Bay decreased, while during drier years sediment flux into Lower South Bay increased. The increase in net-landward sediment flux in WY 2014–2016 occurred as sediment fluxes from local tributaries declined by 75% from 209 kt/year in WY 2009–2011 to 51 kt/year in WY 2014–2016.

An increase in shoal-to-channel sediment flux from enhanced cross-channel density gradients is thought to have caused the increase in net-landward sediment flux in WY 2014–2016. During the drought, decreased freshwater inflow resulted in reduced mixing between the main tidal-channel and extensive shoals. Because freshwater inflow is concentrated in the main tidal channel relative to the shoals, owing to a larger tidal excursion in the main channel, freshwater inflow initially enhances cross-channel density gradients and shoal-to-channel sediment flux. However, if the volume of freshwater inflow replaces approximately more than one-half of the volume of freshwater in the main channel, the cross-channel density gradient is reduced as more-saline shoal water is replaced by incoming freshwater. Although sediment flux into Lower South Bay is dominated by tidal dispersion, changes in shoal-to-channel advective flux driven by changes in the cross-channel density gradient determine the direction of net sediment flux. When shoal-to-channel sediment flux reduces, a persistent landward-increasing suspended-sediment concentration gradient induces net-seaward sediment flux from Lower South Bay. When shoal-to-channel sediment flux increases, increased availability of sediment in the main tidal channel along with a flood-asymmetry in water velocity counteracts the persistent landward-increasing suspended-sediment concentration gradient and induces net-landward sediment flux into Lower South Bay

Additional observational-based studies and modeling of sediment flux on South Bay shoals could be used to confirm the links between freshwater inflow from the Sacramento-San Joaquin Delta, shoal-to-channel sediment flux, and Lower South Bay sediment flux. If confirmed, forecast estimates of freshwater inflow from the Sacramento-San Joaquin Delta may need to be included in tidal marsh sustainability studies that aim to estimate future sediment supply for tidal marshes of Lower South Bay and possibly South Bay. For estuaries exhibiting a channel-shoal bathymetry, with shoal width exceeding the cross-channel tidal excursion, a similar sensitivity of cross-channel sediment flux to freshwater inflow may occur.

Acknowledgments The authors wish to thank the associate editor and two anonymous reviewers whose input improved the readability and content of this manuscript. The authors wish to thank Darin Einhell, Kurt Weidich, Paul Buchanan, Gwen Davies, David Hart, and Selina Davila-Olivera for assistance with data collection.

Funding The Regional Monitoring Program for Water Quality in San Francisco Bay and a San Francisco Bay Water Board enforcement action provided funding for data collection.

References

Bearman, J.A., C.T. Friedrichs, B.E. Jaffe, and A.C. Foxgrover. 2010. Spatial trends in tidal flat shape and associated environmental parameters in South San Francisco Bay. *Journal of Coastal Research* 26 (2): 342–349.

Bever, A.J., M.L. MacWilliams, and D.K. Fullerton. 2018. Influence of an observed decadal decline in wind speed on turbidity in the San Francisco Estuary. *Estuaries and Coasts* 41 (7): 1943–1967.

Boesch, D., E. Burreson, W. Dennison, E. Houde, M. Kemp, V. Kennedy, R. Newell, K. Paynter, R.J. Orth, R. Ulanowicz, and C. Peterson. 2001. Factors in the decline of coastal ecosystems. *Science* 293 (5535) :1589–1591. https://doi.org/10.1126/science.293.5535.1589c.

Brand, A., J.R. Lacy, K. Hsu, D. Hoover, S. Gladding, and M.T. Stacey. 2010. Wind-enhanced resuspension in the shallow waters of South San Francisco Bay: Mechanisms and potential implications for cohesive sediment transport. *Journal of Geophysical Research, Oceans* 115 (C11). https://doi.org/10.1029/2010JC006172.

Buchanan, P.A., M.A. Downing-Kunz, D.H. Schoellhamer, and D.N. Livsey. 2018. Continuous water-quality and suspended-sediment transport monitoring in the San Francisco Bay, California, water years 2014–15, U.S. Geological Survey Fact Sheet 2018-3013 https://doi.org/10.3133/fs20183013.

Caffrey, J.M. 1995. Spatial and seasonal patterns in sediment nitrogen remineralization and ammonium concentrations in San Francisco Bay, California. *Estuaries* 18 (1): 219–233.

California Department of Water Resources. 1986. DAYFLOW computer program documentation and data summary user's guide. Sacramento, California. http://www.water.ca.gov/dayflow/documentation. Accessed 17 June 2020.

Cayan, D., A. Luers, G. Franco, M. Hanemann, and B. Croes. 2008. California at a crossroads: Climate change science informing policy. *Climatic Change* 87.

Chernetsky, A.S., H.M. Schuttelaars, and S.A. Talke. 2010. The effect of tidal asymmetry and temporal settling lag on sediment trapping in tidal estuaries. *Ocean Dynamics* 60 (5): 1219–1241.

Conomos, T.J. 1979. Properties and circulation of San Francisco Bay waters.

Conomos, T.J., R.E. Smith, and J.W. Gartner. 1985. *Environmental setting of San Francisco Bay. In Temporal dynamics of an estuary: San Francisco Bay*, 1–12. Dordrecht: Springer.

Costanza, R., R. d'Arge, R. De Groot, S. Farber, M. Grasso, B. Hannon, K. Limburg, S. Naeem, R.V. O'neill, J. Paruelo, and R.G. Raskin. 1997. The value of the world's ecosystem services and natural capital. *Nature* 387 (6630): 253–260.

Crauder, J., Downing-Kunz, M.A., Hobbs, J.A., Manning, A.J., Novick, E., Parchaseo, F., Wu, J., Schoellhamer, D.H., Senn, D.B., Shellenbarger, G.G., Thompson, J. and Yee, D. 2016. Lower South Bay Nutrient Synthesis. Richmond: San Francisco Estuary Institute & Aquatic Science Center.

D'Alpaos, A., S. Lanzoni, M. Marani, and A. Rinaldo. 2007. Landscape evolution in tidal embayments: Modeling the interplay of erosion, sedimentation, and vegetation dynamics. *Journal of Geophysical Research - Earth Surface* 112 (F1). https://doi.org/10.1029/2006JF000537.

Downing-Kunz, M.A., and D.H. Schoellhamer. 2013. Seasonal variations in suspended-sediment dynamics in the tidal reach of an estuarine tributary. *Marine Geology* 345: 314–326.

Dyer, K.R. 1974. The salt balance in stratified estuaries. *Estuarine and Coastal Marine Science* 2 (3): 273–281.

Dyer, K.R. 1998. *Estuaries: A physical introduction*. 2nd ed, 210. Chichester: Wiley.

Edwards, T.K., G.D. Glysson, H.P. Guy, and V.W. Norman. 1999. *Field methods for measurement of fluvial sediment*, 89. Denver: US Geological Survey.

Elias, E., J. Hansen, and L.H. Erikson. 2013. San Francisco Bay Basic Tide Model. https://doi.org/10.5066/F7DN4330

Fagherazzi, S., M.L. Kirwan, S.M. Mudd, G.R. Guntenspergen, S. Temmerman, A. D'Alpaos, J. Van De Koppel, J.M. Rybczyk, E. Reyes, C. Craft, and J. Clough. 2012. Numerical models of salt marsh evolution: Ecological, geomorphic, and climatic factors. *Reviews of Geophysics* 50 (1). https://doi.org/10.1029/2011RG000359.

Flick, R.E., J.F. Murray, and L.C. Ewing. 2003. Trends in United States tidal datum statistics and tide range. *Journal of Waterway, Port, Coastal, and Ocean Engineering* 129 (4): 155–164.

Fregoso, T.A., R-F. T. Wang, E.S. Ateljevich, and B.E. Jaffe. 2017, A new seamless, high-resolution digital elevation model of the San Francisco Bay-Delta Estuary, California: U.S. Geological Survey Open-File Report 2017–1067, 27 p., https://doi.org/10.3133/ofr20171067.

Ganju, N.K., and D.H. Schoellhamer. 2006. Annual sediment flux estimates in a tidal strait using surrogate measurements. *Estuarine, Coastal and Shelf Science* 69 (1-2): 165–178.

Geyer, W.R., and P. MacCready. 2014. The estuarine circulation. *Annual Review of Fluid Mechanics* 46 (1): 175.

Geyer, W.R., and R.P. Signell. 1992. A reassessment of the role of tidal dispersion in estuaries and bays. *Estuaries* 15 (2): 97–108.

Gostic, M. 2018. Sediment Pathways in San Francisco South Bay. Masters Thesis; TU Delft.

Hager, S.W., and L.E. Schemel. 1996. Dissolved inorganic nitrogen, phosphorus, and silicon in South San Francisco Bay. I. Major factors affecting distributions. In *San Francisco Bay: The Ecosystem, Pacific Division*, ed. J.T. Hollibaugh, 189–215. San Francisco: American Association for the Advancement of Science.

Helsel, D.R., and R.M. Hirsch. 2002. *Statistical methods in water resources*. Vol. 323. Reston: US Geological Survey.

Hill, K., T. Dauphinee, and D. Woods. 1986. The extension of the Practical Salinity Scale 1978 to low salinities. *IEEE Journal of Oceanic Engineering* 11 (1): 109–112.

Huzzey, L.M., J.E. Cioern, and T.M. Powell. 1990. Episodic changes in lateral transport and phytoplankton distribution in South San Francisco Bay. *Limnology and Oceanography* 35 (2): 472–478.

Jackson, J.B.C., M.X. Kirby, W.H. Berger, K.A. Bjorndal, L.W. Botsford, B.J. Bourque, R.H. Bradbury, R. Cooke, J. Erlandson, J.A. Estes, T.P. Hughes, S. Kidwell, C.B. Lange, H.S. Lenihan, J.M. Pandolfi, C.H. Peterson, R.S. Steneck, M.J. Tegner, and R.R. Warner. 2001. Historical overfishing and the recent collapse of coastal ecosystems. *Science* 293 (5530): 629–638.

Jaffe, B. and A.C. Foxgrover. 2006. Sediment deposition and erosion in South San Francisco Bay, California from 1956 to 2005 (p. 20). US Geological Survey.

Kimmerer, W.J. 2002. Physical, biological, and management responses to variable freshwater flow into the San Francisco Estuary. *Estuaries* 25 (6): 1275–1290.

Kirwan, M.L., S. Temmerman, E.E. Skeehan, G.R. Guntenspergen, and S. Fagherazzi. 2016. Overestimation of marsh vulnerability to sea level rise. *Nature Climate Change* 6 (3): 253–260.

Knowles, N., and D.R. Cayan. 2002. Potential effects of global warming on the Sacramento/San Joaquin watershed and the San Francisco estuary. *Geophysical Research Letters* 29 (18): 38–31.

Lacy, J.R., D.H. Schoellhamer and J.R. Burau. 1996. Suspended-solids flux at a shallow-water site in South San Francisco Bay. In Proceedings of the North American water and environment congress.

Lacy, J.R., S. Gladding, A. Brand, A. Collignon, and M. Stacey. 2014. Lateral baroclinic forcing enhances sediment transport from shallows to channel in an estuary. *Estuaries and Coasts* 37 (5): 1058–1077.

Largier, J.L., J.T. Hollibaugh, and S.V. Smith. 1997. Seasonally hypersaline estuaries in Mediterranean-climate regions. *Estuarine, Coastal and Shelf Science* 45 (6): 789–797.

Lerczak, J.A., W.R. Geyer, and R.J. Chant. 2006. Mechanisms driving the time-dependent salt flux in a partially stratified estuary. *Journal of Physical Oceanography* 36 (12): 2296–2311.

Levesque, V.A. and K.A. Oberg. 2012. Computing discharge using the index velocity method (pp. 3-A23). US Department of the Interior, US Geological Survey.

Livsey, D.N., Downing-Kunz, M.A., Schoellhamer, D.H. and Manning, A.J., 2020. Suspended sediment flux in the San Francisco Estuary: Part I—Changes in the vertical distribution of suspended sediment and bias in estuarine sediment flux measurements. *Estuaries and Coasts*, pp. 1–17.

Lotze, H.K., H.S. Lenihan, B.J. Bourque, R.H. Bradbury, R.G. Cooke, M.C. Kay, S.M. Kidwell, M.X. Kirby, C.H. Peterson, and J.B.C. Jackson. 2006. Depletion, degradation, and recovery potential of estuaries and coastal seas. *Science* 312 (5781): 1806–1809.

Love, A.H., B.K. Esser, and J.R. Hunt. 2003. Reconstructing contaminant deposition in a San Francisco Bay marine, California. *Journal of Environmental Engineering* 129 (7): 659–666.

McCulloch, D.S., D.H. Peterson, P.R. Carlson and T.J. Conomos. 1970. A preliminary study of the effects of water circulation in the San Francisco Bay estuary: A. Some effects of fresh-water inflow on the flushing of south San Francisco Bay, B. Movement of seabed drifters in the San Francisco Bay estuary and the adjacent Pacific Ocean (No. 637-A, B). US Geological Survey.

McKee, L.J., M. Lewicki, D.H. Schoellhamer, and N.K. Ganju. 2013. Comparison of sediment supply to San Francisco Bay from watersheds draining the Bay Area and the Central Valley of California. *Marine Geology* 345: 47–62.

NOAA, National Geophysical Data Center. 2010: San Francisco Bay, California 1/3 arc-second NAVD 88 Coastal Digital Elevation Model. NOAA National Centers for Environmental Information. https://data.nodc.noaa.gov/cgi-bin/iso?id=gov.noaa.ngdc.mgg.dem:741#. Accessed June, 17, 2020.

NOAA, National Ocean Servce. 1998. *Medium Resolution Digital Vector Shoreline*. https://shoreline.noaa.gov/data/datasheets/medres.html. Accessed 17 June 2020.

NOAA. 2019. Vertical datum transformation, VDatum 4.0.1, https://vdatum.noaa.gov/. Accessed June, 18, 2020.

Pond, S., and G.L. Pickard. 1983. *Introductory dynamical oceanography*. Oxford: Butterworth-Heinemann Ltd..

Powell, T.M., J.E. Cloern, and L.M. Huzzey. 1989. Spatial and temporal variability in South San Francisco Bay (USA). I. Horizontal distributions of salinity, suspended sediments, and phytoplankton biomass and productivity. *Estuarine, Coastal and Shelf Science* 28 (6): 583–597.

Pubben, S.G.T. 2017. 3D Mixing patterns in San Francisco South Bay. Masters Thesis; TU Delft.

Robeson, S.M. 2015. Revisiting the recent California drought as an extreme value. *Geophysical Research Letters* 42 (16): 6771–6779.

Ruhl, C.A., and M.R. Simpson. 2005. *Computation of discharge using the index-velocity method in tidally affected areas*, 1–41. Denver: US Department of the Interior, US Geological Survey.

Rustomji, P., and S.N. Wilkinson. 2008. Applying bootstrap resampling to quantify uncertainty in fluvial suspended sediment loads estimated using rating curves. *Water Resources Research* 44 (9). https://doi.org/10.1029/2007WR006088.

Schettini, C.A., A. Valle-Levinson, and E.C. Truccolo. 2017. Circulation and transport in short, low-inflow estuaries under anthropogenic stresses. *Regional Studies in Marine Science* 10: 52–64.

Schoellhamer, D.H. 1996. Factors affecting suspended-solids concentrations in south San Francisco Bay, California. *Journal of Geophysical Research, Oceans* 101 (C5): 12087–12095.

Schoellhamer, D.H. 2011. Sudden clearing of estuarine waters upon crossing the threshold from transport to supply regulation of sediment transport as an erodible sediment pool is depleted: San Francisco Bay, 1999. *Estuaries and Coasts* 34 (5): 885–899.

Schoellhamer, D.H., T.E. Mumley, and J.E. Leatherbarrow. 2007. Suspended sediment and sediment-associated contaminants in San Francisco Bay. *Environmental Research* 105 (1): 119–131.

Shellenbarger, G.G., and D.H. Schoellhamer. 2011. Continuous salinity and temperature data from San Francisco Estuary, 1982–2002: Trends and the salinity–freshwater inflow relationship. *Journal of Coastal Research* 27 (6): 1191–1201.

Shellenbarger, G.G., S.A. Wright, and D.H. Schoellhamer. 2013. A sediment budget for the southern reach in San Francisco Bay, CA: Implications for habitat restoration. *Marine Geology* 345: 281–293.

Stralberg, D., M. Brennan, J.C. Callaway, J.K. Wood, L.M. Schile, D. Jongsomjit, M. Kelly, V.T. Parker, and S. Crooks. 2011. Evaluating tidal marsh sustainability in the face of sea-level rise: A hybrid modeling approach applied to San Francisco Bay. *PLoS One* 6 (11). https://doi.org/10.1371/journal.pone.0027388.

Swanson, K.M., J.Z. Drexler, D.H. Schoellhamer, K.M. Thorne, M.L. Casazza, C.T. Overton, J.C. Callaway, and J.Y. Takekawa. 2014. 2014. Wetland accretion rate model of ecosystem resilience (WARMER) and its application to habitat sustainability for endangered species in the San Francisco Estuary. Estuaries and Coasts, 37(2), pp.476-492. Species in the San Francisco Estuary. *Estuaries and Coasts* 37 (2): 476–492.

U.S. Geological Survey, 2020. *National Water Information System: U.S. Geological Survey web interface*. https://doi.org/10.5066/F7P55KJN. Accessed 17 June 2020.

van Kempen, O. 2017. Sediment pathways in San Francisco South Bay. Masters Thesis; TU Delf.t

Walters, R.A., R.T. Cheng, and T.J. Conomos. 1985. *Time scales of circulation and mixing processes of San Francisco Bay waters. In Temporal dynamics of an estuary: San Francisco Bay*, 13–36. Dordrecht: Springer.

Work, P.A., M.A. Downing-Kunz, and D. Livsey. 2017. Record-high specific conductance and water temperature in San Francisco Bay during water year 2015: U.S. Geological Survey Open-File Report 2017–1022, 4 p. https://doi.org/10.3133/ofr20171022.